NAVAL POSTGRADUATE SCHOOL
Monterey, California

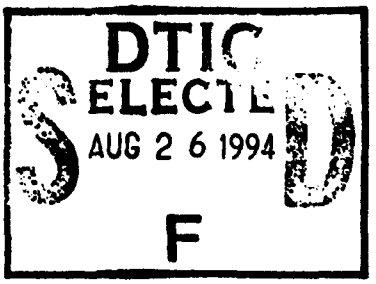

THESIS

SODIUM SULFATE CORROSION OF SILICON CARBIDE FIBER-REINFORCED CALCIUM ALUMINOSILICATE GLASS-CERAMIC MATRIX COMPOSITES

by

Peter J. Newton

March, 1994

Thesis Advisor: Alan G. Fox

REPORT DOCUMENTATION PAGE

Form Approved OMB No. 0704

1. AGENCY USE ONLY	2. REPORT DATE	3. REPORT TYPE AND DATES COVERED
	March 1994	Master's Thesis

4. TITLE AND SUBTITLE Sodium Sulfate Corrosion of Silicon Carbide Fiber-Reinforced Calcium Aluminosilicate Glass-Ceramic Matrix Composites

5. FUNDING NUMBERS

6. AUTHOR(S) *Peter John Newton*

7. PERFORMING ORGANIZATION NAME(S) AND ADDRESS(ES)
Naval Postgraduate School
Monterey, CA 93943-5000

8. PERFORMING ORGANIZATION REPORT NUMBER

9. SPONSORING/MONITORING AGENCY NAME(S) AND ADDRESS(ES)
Naval Surface Warfare Center
Warminster, PA 18974

10. SPONSORING/MONITORING AGENCY REPORT NUMBER

11. SUPPLEMENTARY NOTES The views expressed in this thesis are those of the author and do not reflect the official policy or position of the Department of Defense or the U.S. Government.

12a. DISTRIBUTION/AVAILABILITY STATEMENT
Approved for public release; distribution is unlimited.

12b. DISTRIBUTION CODE
*A

13.

ABSTRACT Hot corrosion effects of Sodium Sulfate (Na_2SO_4) coated Calcium Aluminosilicate (CAS)/Silicon Carbide (SiC) reinforced glass-ceramic matrix composite were investigated using Scanning Electron Microscopy (SEM), Energy Dispersive X-ray Analysis (EDX) and X-ray Diffraction (XRD). The samples provided by the Naval Air Warfare Center (NAWC) were unidirectional SiC/CAS as follows: (1) as received, (2) uncoated in air, (3) Na_2SO_4 coated in air and (4) Na_2SO_4 coated in argon. A heat treatment was conducted at 900 °C for 100 hours. Experimental observations indicated that the Na_2SO4 coating in an oxidising environment had severely corroded the silicon fiber resulting in a silica rich, Nepheline ($NaAlSiO_4$), Wollastonite ($CaSiO_3$), Rankinite ($Ca_3Si_2O_7$), Albite ($NaAlSi_3O_8$) and glassy phases. In the argon atmosphere fiber degradation was present although less severe than in the oxygen environment. Similar phases of silica rich, Nepheline, Albite, Rankinite, Mullite ($Al_6Si_2O_{13}$), Pseudo-Wollastonite ($CaSiO_3$) and a glassy region were present. Minimal fiber and matrix degradation was observed in the uncoated sample heat treated in air.

14. SUBJECT TERMS Calcium Aluminosilicate, SiC Fiber Reinforced Composites

15. NUMBER OF PAGES 81

16. PRICE CODE

17. SECURITY CLASSIFICATION OF REPORT	18. SECURITY CLASSIFICATION OF THIS PAGE	19. SECURITY CLASSIFICATION OF ABSTRACT	20. LIMITATION OF ABSTRACT
Unclassified	Unclassified	Unclassified	UL

NSN 7540-01-280-5500

Standard Form 298 (Rev. 2-89)
Prescribed by ANSI STD. 239-18

Approved for public release; distribution is unlimited.

Sodium Sulfate Corrosion of Silicon Carbide Fiber-Reinforced Calcium Aluminosilicate Glass-Ceramic Matrix Composites

by

Peter J. Newton
Lieutenant, United States Navy
B.E., State University of New York Maritime College, 1986

Submitted in partial fulfillment
of the requirements for the degree of

MASTERS OF SCIENCE IN MECHANICAL ENGINEERING
from the

NAVAL POSTGRADUATE SCHOOL
March 1994

Author: 
Peter J. Newton

Approved by: 
Alan G. Fox, Thesis Advisor


Matthew D. Kelleher, Chairman
Department of Mechanical Engineering

ABSTRACT

Hot corrosion effects of Sodium Sulfate (Na_2SO_4) coated Calcium Aluminosilicate (CAS)/Silicon Carbide (SiC) reinforced glass-ceramic matrix composite were investigated using Scanning Electron Microscopy (SEM), Energy Dispersive X-ray Analysis (EDX) and X-ray Diffraction (XRD). The samples provided by the Naval Air Warfare Center (NAWC) were unidirectional SiC/CAS as follows: (1) as received, (2) uncoated in air, (3) Na_2SO_4 coated in air and (4) Na_2SO_4 coated in argon. A heat treatment was conducted at 900 °C for 100 hours. Experimental observations indicated that the Na_2SO4 coating in an oxidising environment had severely corroded the silicon fiber resulting in a silica rich, Nepheline ($NaAlSiO_4$), Wollastonite ($CaSiO_3$), Rankinite ($Ca_3Si_2O_7$), Albite ($NaAlSi_3O_8$) and glassy phases. In the argon atmosphere fiber degradation was present although less severe than in the oxygen environment. Similar phases of silica rich, Nepheline, Albite, Rankinite, Mullite ($Al_6Si_2O_{13}$), Pseudo-Wollastonite ($CaSiO_3$) and a glassy region were present. Minimal fiber and matrix degradation was observed in the uncoated sample heat treated in air.

TABLE OF CONTENTS

LIST OF TABLES

LIST OF FIGURES

ACKNOWLEDGEMENTS

I would like to personally thank Professor Alan G. Fox for his guidance and assistance in helping me prepare this thesis. Without his personal attention and support the extent of my thesis research would not have been complete. You'll not find a better thesis advisor.

I dedicate this thesis to my family who have supported my many long hours of study at the Naval Postgraduate School. To my sons Tyler and Ryan. A very special thanks to Elizabeth, my lovely wife, who has unselfishly supported me throughout my thesis research and Naval career.

I. INTRODUCTION

The current design of U.S. Naval gas turbine engines utilizes nickel-based superalloys in the manufacturing of engine components. This superalloy has a high density which subsequently creates high stresses during engine operation. The use of superalloys reduces engine efficiency, increases weight requirement (reducing thrust to weight ratios) and thus production costs. This study provides the basis for the introduction of the SiC fiber-reinforced calcium aluminosilicate (SiC/CAS) composites into the production of turbine engine components. This SiC/CAS composite could potentially increase the efficiency of Naval gas turbine engines through elevating the sustainable operating temperatures and reducing weight through the use of low density ceramic composites. The SiC fiber reinforcement increases the strength and toughness thus preventing embrittlement at elevated temperatures as occurs in the monolithic ceramic. The specific strength for ceramics and superalloys is represented in Figure 1.

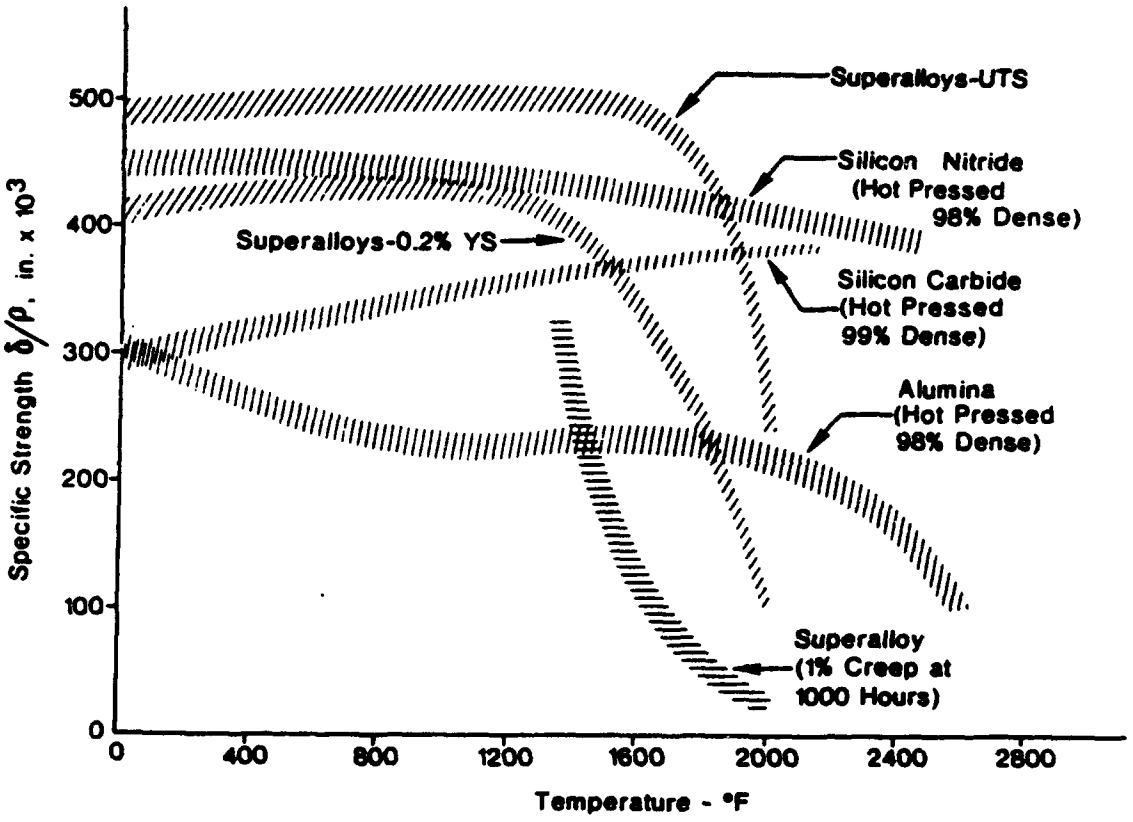

Figure 1. Specific Strength Comparison of Ceramics and Superalloys [Ref. 1: pg. 219]

The relatively low coefficient of thermal expansion and corrosion resistance will further enhance engine performance and reliability.

Naval aircraft inherently operate in hostile environments under constantly changing operating conditions. The versatility of the aircraft requires they operate in sodium (from sea air) and sulfur (from fuels) atmospheres which result in the formation of sodium sulfate (Na_2SO_4) salt deposits on engine component surfaces. These salts combined with elevated temperatures can lead to hot corrosion effects resulting in degradation of the SiC/CAS composite. At elevated temperatures the salt forms sodium oxide (Na_2O), which diffuses into the composite, leading to the degradation of the glass-ceramic matrix and SiC fibers, and deterioration of the mechanical properties.

The SiC/CAS system exhibits good high temperature oxidation resistance without significant degradation of material properties. The hot corrosion of the composite in the presence of Na_2SO_4 is not yet fully understood. A complete study is essential before the introduction of ceramic composites into engine component production.

The intent of this study is to show the hot corrosion effects of Na_2SO_4 salted coated SiC/CAS with respect to microstructure and chemical composition.

II. BACKGROUND

A. GLASS CERAMICS

Ceramic glass-matrices (not reinforced) consist of the combination of one or more metallic oxides such as Li_2O and CaO in combination with alumina and silica. In general the morphology of the matrix is a crystalline structure which may also include amorphous glassy phases. Ceramic matrices characteristically have strong ionic bonds which lead to low failure strains, toughness, thermal/mechanical shock resistance, tensile strengths, yet tend to exhibit high elastic moduli and temperature resistance. When the composite is formed through fiber reinforcement, there is a noticeable increase in strength, toughness, stiffness at elevated temperatures, chemical inertness and a lower density. Material properties are controlled through uniform grain size refinement, fiber/matrix volume fraction ratio, fiber matrix bond strength and relative amount of crystalline to glass phases.

The calcium aluminosilicate glass-ceramic composite (CAS) studied in the present work , (39.5 wt% SiO_2, 18.5 wt% CaO, 38.5 wt% Al_2O_3, 0.5 wt% As_2O_3 and 3.0 wt% ZrO_2) contains approximately 38 vol % standard Nicalon (Nippon Co.) fiber (15 μm diameter).

The mechanical properties of the matrix and reinforced matrix are shown in Table I.

TABLE I. MECHANICAL PROPERTIES [Ref. 2: pg. 3, Ref. 7: pg. 106]

MAT'L PROPERTIES	CAS MATRIX	SiC/CAS COMPOSITE
ELASTIC MODULUS (GPa)	98	124.1
TENSILE STRENGTH (MPa)	124	503
DENSITY (G/CM^3)	2.76	2.70
COEFFICIENT OF THERMAL EXPANSION ($x\ 10^{-6}\ °C^{-1}$)	5.0	4.0
MAXIMUM TEMPERATURE (°C)	1350	1300-1350

The predominant crystalline phase in the matrix is anorthite ($CaAl_2Si_2O_6$). [Ref. 2: pg. 3]

The major limiting factor in ceramic composite application is the embrittlement mechanism at room temperature. This brittle behavior is both nonlinear and inelastic once a relatively low stress state is achieved. This embrittlement

is predominantly due to the small number of slip systems which impedes dislocation motion and the requirement to break strong ionic bonds in order for slip to occur [Ref. 3]. Upon crack initiation within the matrix it is free to propagate, due to the inelasticity of the matrix, until it is blunted by a fiber or failure occurs.

B. THE CALCIUM ALUMINOSILICATE SYSTEM

The ternary phase diagram of the calcium aluminosilicate system which will be studied in the present work is shown in Figure 2.

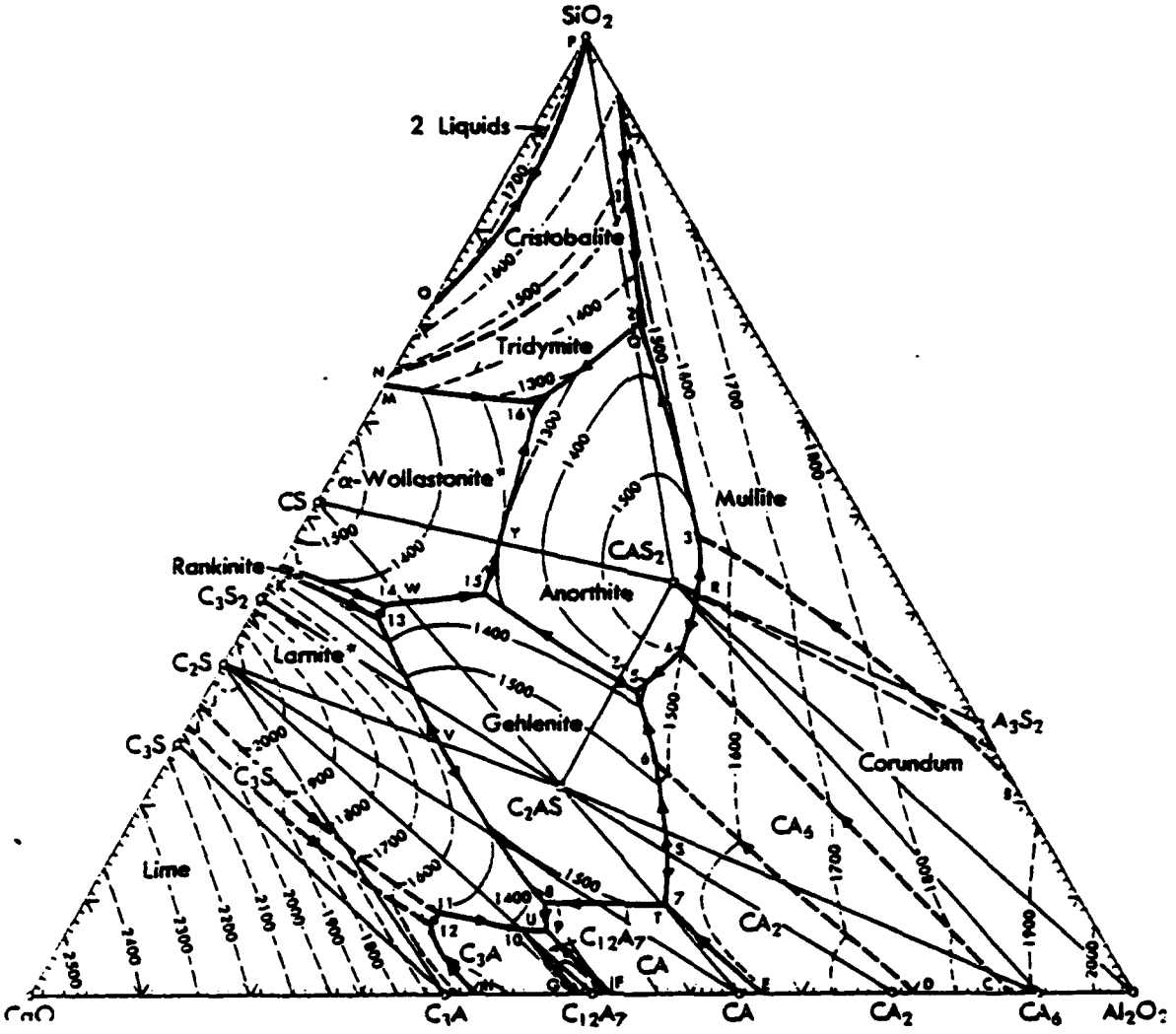

Figure 2. CAS Phase Diagram [Ref. 4: pg. 313]

CAS is usually manufactured so that the primary crystalline phase is anorthite with a triclinic crystal structure. Small amounts ZrO_2 (3 wt%) are often added to generate crystallites (~ 5 nm in diameter) that act as nucleation sites for crystal growth. In addition the ZrO_2 reduces glass viscosity and lowers the activation energy for crystallization. [Ref. 5: pg. 2818] Small amounts (0.5 wt%) of As_2O_3 can significantly increase the basicity of the matrix. The addition of such small amounts of ZrO_2 and As_2O_3 does not apparently lead to any additional crystalline phases within the anorthite matrix.

The major effect on the activity of silica in a glass-ceramic matrix is the addition of oxide components, such as As_2O_3, which serve to make the matrix more basic. This basicity controls the degree of polygonization, which is the formation of sub boundaries leading to climb whereby an edge dislocation changes from horizontal to vertical in orientation at cell walls. This polygonization greatly effects dislocation motion and hence plastic strength of the matrix. Basic silicates have a high density of ionic bonds, are poorly polygonized, good oxidizers and have enhanced solubility of carbon oxide gases (CO and CO_2). As the matrix basicity increases so does the oxidation potential however it may also cause embrittlement due to the impedance of dislocation motion. Acidic silicates on the other hand have a high density of covalent bonds, are highly polygonized and are

quite reducing. This lowers the matrix oxidation potential but improves the resistance to embrittlement. [Ref. 6: pg. 3148]

The mechanical properties of a monolithic CAS sample are presented in Table I.

C. SIC FIBER-REINFORCED CALCIUM ALUMINOSILICATE COMPOSITES

With the incorporation of the SiC fiber reinforcement to the CAS matrix, the maximum sustainable temperature in combination with the increased structural stability, makes the composite very favorable for gas turbine component applications. The SiC/CAS composite, when compared to the monolithic CAS, displays an appreciable ductility, higher toughness, higher strength and therefore an increase in the resistance to brittle catastrophic failure. The Nicalon SiC fiber's material properties are as follows: elastic modulus 193.2 Gpa, tensile strength 2760 Mpa, coefficient of thermal expansion $4.0 \times 10^{-6}\ °C^{-1}$, density 2.55 g/cm^3, average fiber diameter 10-20 μm and a maximum use temperature of 1300 °C [Ref. 7: pg. 5485]. The resulting composite has an elastic modulus of 124.1 Gpa and a tensile strength of 503 Mpa.

A typical stress-strain curve for the $[0°]_8$ SiC/CAS composite is presented in Figure 3.

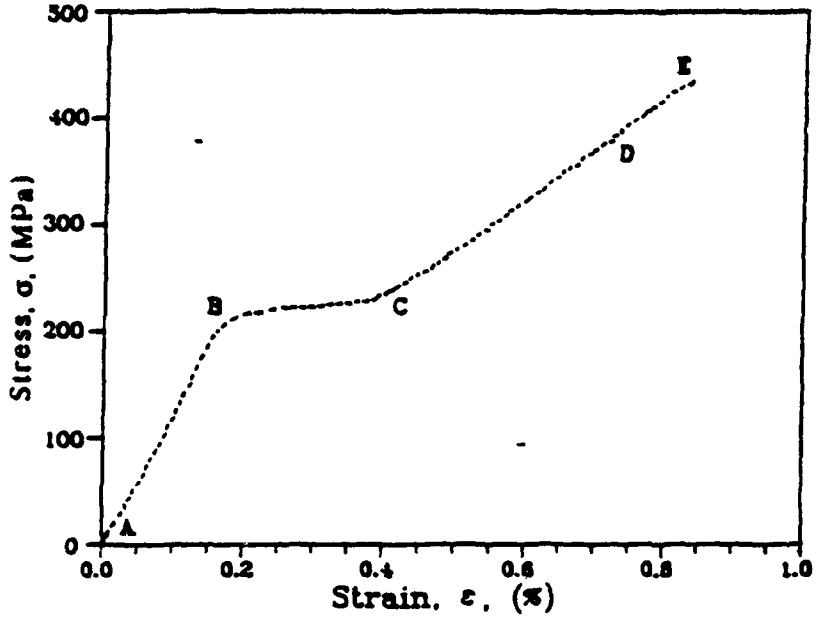

Figure 3. Stress vs Strain Plot for $[0°]_8$ SiC/CAS Composite [Ref. 8: pg. 107]

The characteristic features representative of the failure mechanisms and processes are displayed in Figure 3. The linear portion between A and B represents the elastic behavior of the composite before any microfailures occur. At point B the plot becomes non-linear which indicates the onset of transverse matrix cracking and fiber/matrix debonding. The region between B and C represents the multiplication of transverse cracking. The quasi-linear region with increasing slope between C and E represents a region where no further matrix failure occurs and the onset of fiber failure occurs until fracture. [Ref. 8: pg. 107]

The mechanism of load transfer accounts for the strengthening of the composite by the SiC fibers. The fibers (high modulus), which are the load bearing components, are chemically bonded to the matrix (low modulus) which transfers the load as indicated in Figure 4.

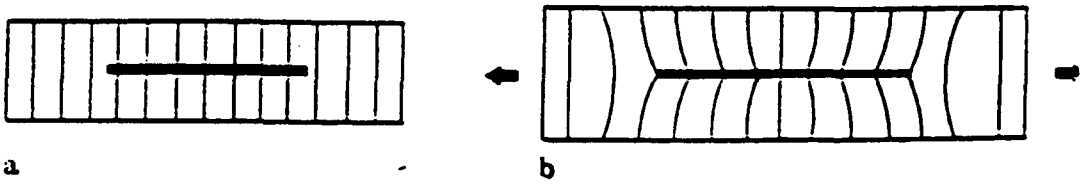

Figure 4. A High-Modulus Fiber Embedded in a Low-Modulus Matrix: a Before Deformation, b After Deformation [Ref. 9: pg. 198]

As depicted in Figure 3, no direct loading of the fiber occurs and the fiber and the matrix locally experience different axial displacements due to their difference in elastic moduli. [Ref. 9: pg. 198]

The mechanism of load transfer is governed by the matrix to fiber interfacial strength. This is represented in the tensile load vs displacement curve in Figure 5. The failure

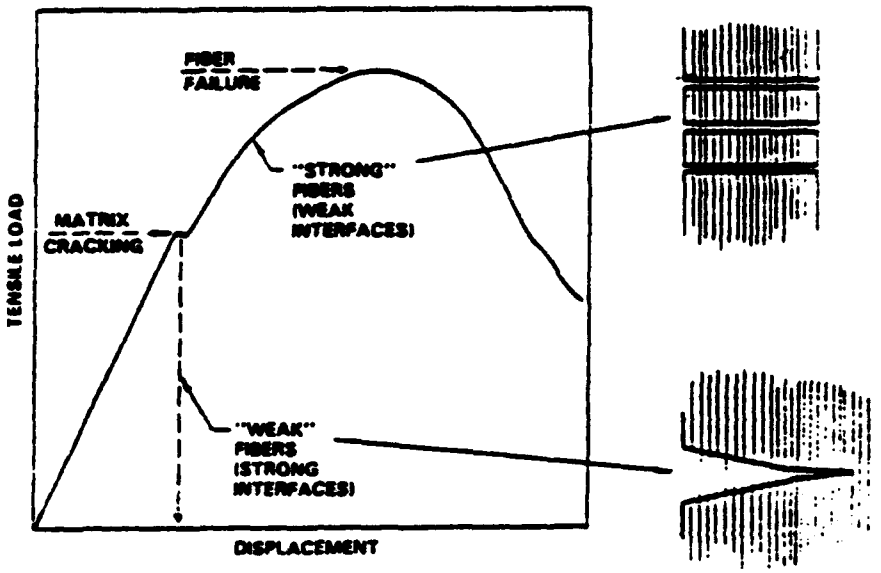

Figure 5. A Tensile Stress-Strain Curve for a Tough Ceramic Composite. [Ref. 10: pg. 2570]

mechanism desired is that of a weak interfacial strength where a propagating crack is blunted by the fiber, fiber matrix debonding occurs and fiber bridging results. The weak fiber interface increases the toughness as the crack now propagates through matrix and not through the brittle fiber. As the crack propagates through the matrix, energy is absorbed by the matrix thus increasing the maximum sustainable tensile load

prior to failure. The effect of fiber bridging on the brittle reinforcement of the matrix is represented in Figure 6.

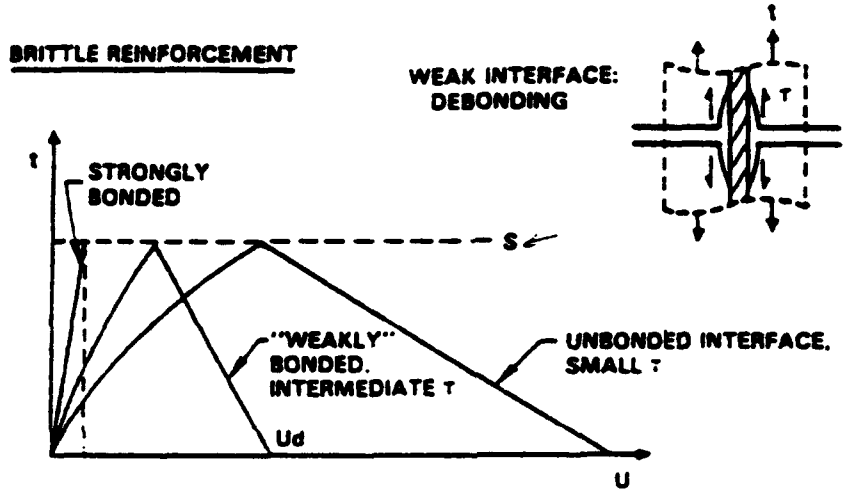

Figure 6. A Schematic Illustrating Various Trends in Crack Openings With Stress [Ref. 10: pg. 2570]

The weak interface requires a much larger crack for fiber failure to occur than in the strong interface thus reducing the brittle effect of the composite. The unbonded interface is not considered. [Ref. 10: pg. 2570] Figure 7 shows crack blunting by SiC fibers.

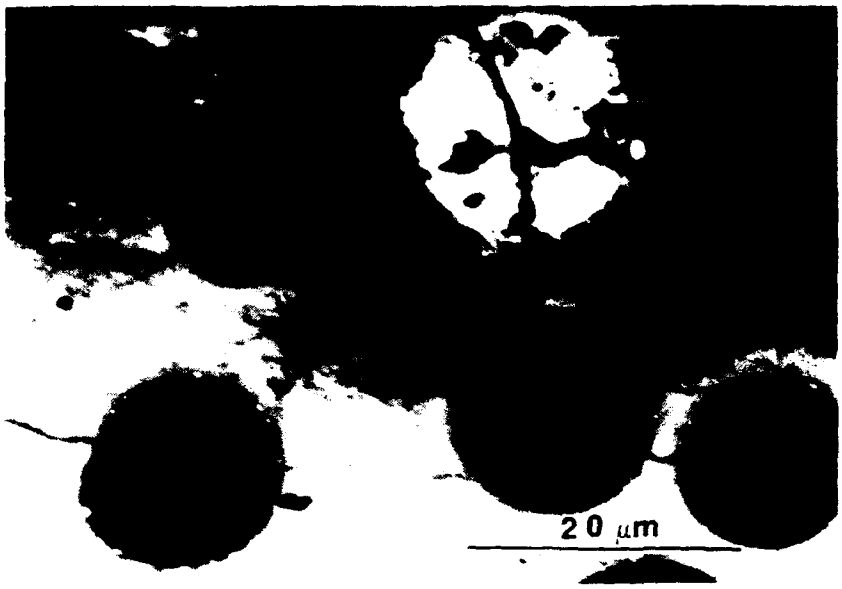

Figure 7. Crack Blunting by SiC Fibers in CAS Composite in Salt Coated Sample Heat Treated in Argon to 900° C

The SiC fiber/CAS matrix interface reaction produces an interfacial structure which satisfies required mechanical response of matrix microcracking and non-catastrophic failure. This reaction layer is a combination of silicate matrix chemistry and non-stoichiometric/non-crystalline fiber structures. The reaction produces a carbon rich layer through the oxidation of SiC by the following reaction: $SiC + O_2 = SiO_2 + C$. The carbon is graphitic in form and serves to provide a diffusion barrier, against gaseous oxygen (O_2), which prevents the oxidation and further degradation of the fiber. Consequent degradation would decrease the composite

strength. The reaction interface layer is presented in Figure 8. [Ref 11: pg. 233]

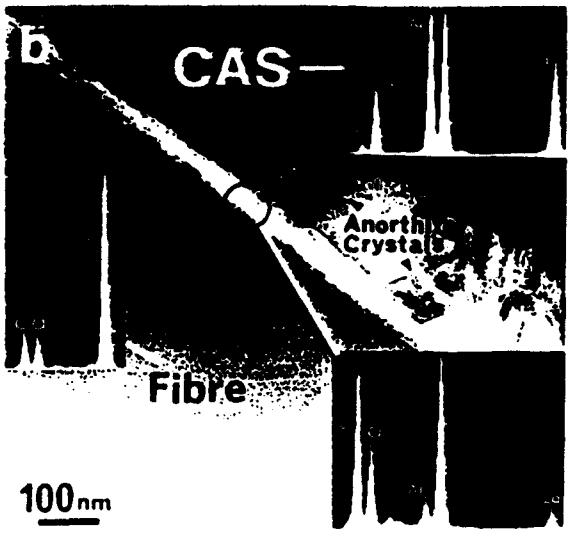

Figure 8. Interface Microanalysis (EDS) in Glass Ceramic/Nicalon Fiber CMC's for CAS Matrix [Ref. 11: pg. 239]

D. CORROSION OF SIC/CAS COMPOSITE BY NA_2SO_4

The SiO_2 layer that forms during processing as a result of a matrix/fiber chemical reaction serves to protect the fiber against further oxidation and degradation. In fuel rich atmospheres, such as in a gas turbine engine, the fiber can be oxidized by the following reaction:

$$SiC_{(s)} + 1.5\ O_2 = SiO_{2(s)} + CO_{(g)}$$

In common oxides, SiO_2 has the lowest permeability to oxygen. The mobile species in the oxidation of SiC is commonly accepted to be oxygen rather than silicon. This leads to the possibility of chemical reactions occurring at the SiO_2 and SiC interfaces. Molecular oxygen diffuses through SiO_2 as interstitials or by network exchange of ionic oxygen. The diffusion coefficient of molecular oxygen is significantly greater then that of ionic oxygen (10^6 times), hence oxygen transport is most likely to occur by molecular oxygen diffusion.[Ref. 2: pg. 5]

The combustion process involves the oxidation of fuels into stable products of carbon dioxide (CO_2) and water (H_2O). Gas turbine engines operate in fuel rich regions (fuel to air ratio greater than one) which produce large amounts of oxygen in the fuel stabilization process. During this process the oxidation of SiC is much faster in wet O_2 vice dry as H_2O has a higher solubility in SiO_2 ($\sim 3.4 \times 10^{19}$ molecules/cm_2) than molecular oxygen in SiO_2 ($\sim 5.5 \times 10^6$ molecules/cm_2). This

rapid diffusion of H_2O molecules leads to rapid oxidation of SiC. [Ref. 13: pg. 3770]

The fuel stabilization process produces corrosion products namely a stable salt, sodium sulfate (Na_2SO_4), which forms from sulfur containing fuels reacting with airborne salts from marine environments.

$$2NaCl_{(s)} + SO_2(g) + .5O_2 + H_2O = Na_2SO_4(l) + 2HCl_{(g)}$$

The salt is deposited on engine components and hot corrosion occurs in a limited temperature range as displayed in Figure 9.

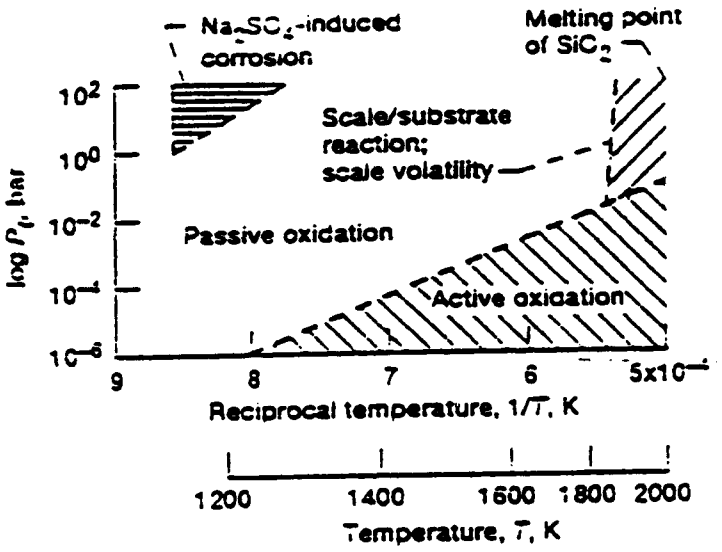

Figure 9. Types of Corrosive Attack and Degradation as an Approximate Function of Reciprocal Temperature [Ref. 12: pg. 6]

Sodium sulfate acts as a corrosive agent between it's melting point 884 °C and up to it's dew point 1000 °C (at one atm), which is dependent upon the partial pressure as

presented in Figure 10 [Ref. 12: pg. 6]. The acidity/bacisity of sodium oxide, which can result from the following equation:

$$Na_2SO_4 = Na_2O + SO_3 = Na_2O + SO_2 + .5\ O_2$$

is also a function of the partial pressure. A high $P(SO_3)$ yields a low Na_2O activity (acidic salt) where as a low $P(SO_3)$ sets a high Na_2O activity (basic salt). [Ref. 14: pg. 2903]

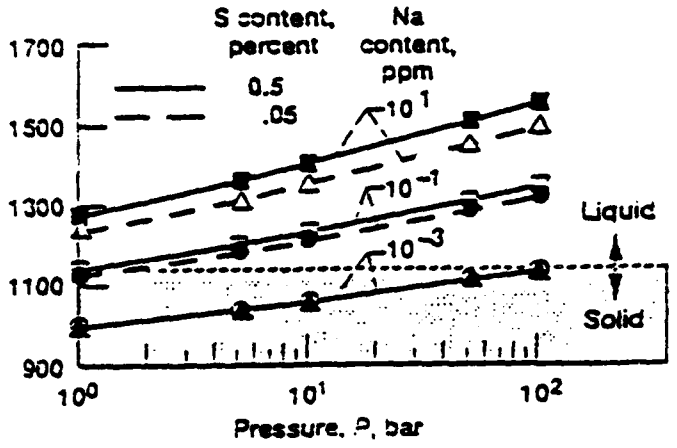

Figure 10. Dewpoints for Na_2SO_4 [Ref. 12: pg. 20]

The SiC/CAS composite is being considered for application in the divergent flaps and seals in the gas turbine convergent/divergent nozzle exhaust system. This engine component experiences temperatures between 650-1100 °C, which is well within the corrosive region depicted in Figure 9 and

is the driving interest for hot corrosion research of this composite.

Within the operating temperatures of the gas turbine engine the Na_2SO_4 deposit is a molten liquid which breaks down into sodium oxide and sulfur trioxide by the following equation:

$$SiO_2 + Na_2SO_4 = Na_2O \cdot (SiO_2) + SO_3$$

Further reactions with the CAS matrix can be as follows:

$$Na_2SO_4 + CaAl_2Si_2O_8 + SiO_2 = 2NaAlSiO_4 + CaSiO_3 + SO_3$$

The SO_3 gas evolves and may form bubbles in the new phases of sodium aluminosilicate and calcium silicate. Consequently as the protective layer is degraded the fiber further oxidizes and substantial fiber degradation occurs leading to a loss of mechanical properties. [Ref. 2: pg. 5]

Previous work by Wang, Kowalik, and Sands on sodium sulfate corrosion of SiC/CAS has indicated an approximate 25% reduction in tensile strengths of samples coated with salt and heat treated to 900 °C in air. Figure 11 provides an experimental stress-strain plot for as received, heat treated, salt/heat treated in air and salt/heat treated in argon. Fiber degradation was substantial in the sample coated/heat treated in air hence a loss of tensile strength however a loss

of less than 10% of it's tensile strength was observed in the sample coated and treated in argon. This indicates that the fiber degradation was less severe in the argon atmosphere. [Ref 15,pg. 11]

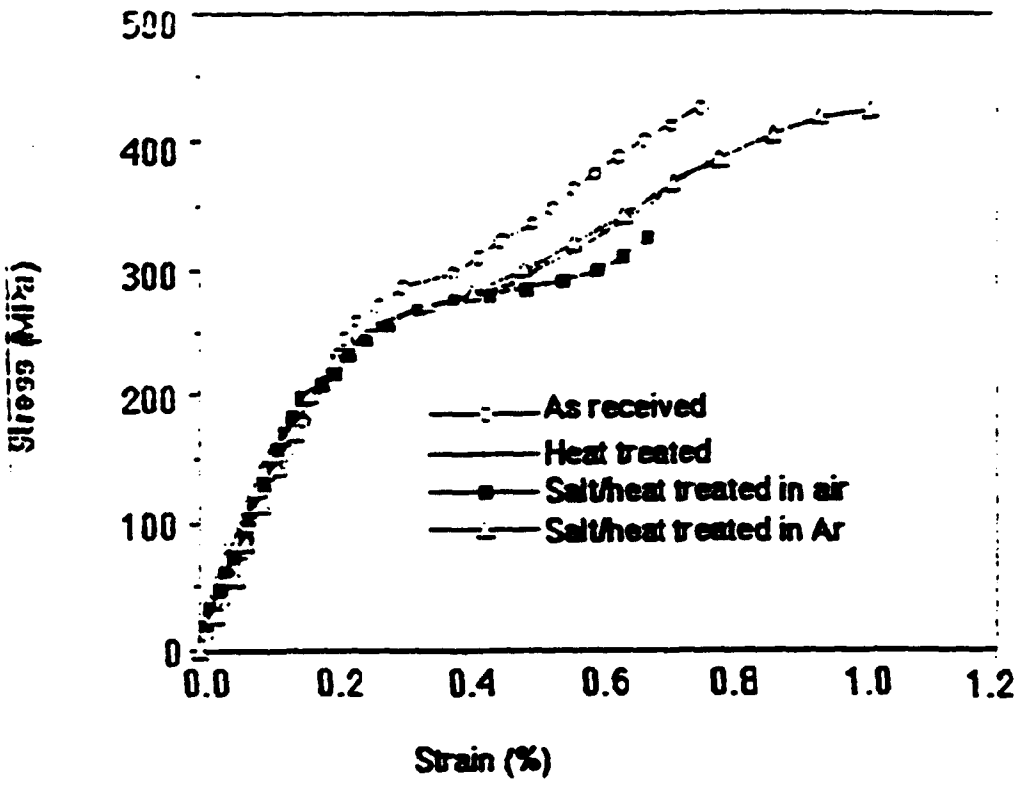

Figure 11. Stress Strain Curves of SiC/CAS Tensile Specimens that were Exposed in Varying Environments [Ref. 15: pg. 11]

III. SCOPE OF PRESENT WORK

In reviewing background literature concerning the hot corrosion of SiC/CAS by sodium sulfate salt deposits, it is seen that if the proper conditions exist then the rapid oxidation of the SiC fibers and the degradation of the matrix occurs. This leads to the deterioration of the composite's mechanical properties.

The present work involves the analysis of the chemical and microstructural changes in the SiC/CAS glass-ceramic matrix composite when exposed to sodium sulfate and heat treated to 900 °C in both air and argon. The samples analyzed were provided by the Naval Air Warfare Center (NAWC) and were as follows: (1) as received SiC/CAS, (2) SiC/CAS heat treated to 900 °C in air, (3) SiC/CAS salt coated and heat treated to 900 °C in air, (4) SiC/CAS salt coated and heat treated to 900 °C in argon. Analysis was performed using the Scanning Electron Microscope (SEM) and X-ray Diffractometer (XRD).

IV. EXPERIMENTAL PROCEDURE

The cerammed SiC/CAS composite was fabricated by Corning Incorporated. Figure 12 shows a schematic of the fabrication process.

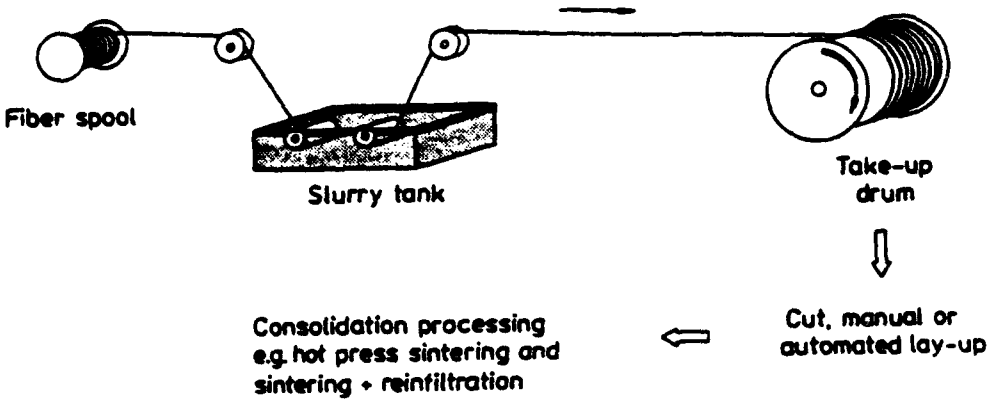

Figure 12. Schematic of Slurry Infiltration Process [Ref. 9: pg. 135]

The fabrication process was as follows:

1. The Nicalon SiC fibers are impregnated by an unconsolidated CAS matrix through a slurry infiltration process. The CAS glass powder contains SiO_2, CaO, Al_2O_3, As_2O_3 and ZrO_2 which were melted, mixed and quenched to form a solid. This solid was then ground into fine particles and mixed with a carrier liquid and organic binder. The ZrO_2 and As_2O_3 where minor matrix constituents added as nucleating and glass fining agents. The SiC fibers were uncoated.

2. The impregnated yarn (SiC fibers and CAS matrix) was carefully wound on a take-up drum.

3. SiC/CAS ribbons where then dried, removed from the drum and cut into predetermined shapes.

4. Eight plys of the ribbon were staked and placed into a furnace to burn off the organic binders.

5. The plys were then hot pressed together under pressure.

6. The dense SiC/CAS composite was then cerammed (Partially crystallized)

The samples where provided by Dr. S. Wang, Naval Air Warfare Center, Warminster PA, were as follows:

1. as received

2. as received and heat treated for 100 hours at 900 °C in air.

3. salt coated and heat treated for 100 hours at 900 °C in air.

4. salt coated and heat treated for 100 hours at 900 °C in argon.

Energy dispersive x-ray analysis was initially performed on the as received sample to determine the preheat treatment phases. The tensile specimen coupon was cut to form a 150 mm by 150 mm SiC/cas composite panel and then coated with

approximately 3.0 mg/cm^2 of sodium sulfate. This coating is equivalent to what is expected to exist on gas turbine engine components after 500 hours of operation at 900 °C with a sulfur fuel impurity of .05%. The coupons were heat treated in air and argon at 900 °C (15 °C/min ramp) for 100 hours. [Ref. 15: pg. 2]

The coated samples were examined to evaluate microstructural and chemical composition changes due to hot corrosive environments. The composition of the as received SiC/CAS glass-ceramic sample is as provided in Table II. The SiC/CAS composition was provided to NAWC by Corning Incorporated. [Ref. 16]

TABLE II SiC/CAS AS RECEIVED MATRIX COMPOSITION

Oxide Components	Composition (wt%)
CaO	18.5
Al_2O_3	38.5
SiO_2	39.5
ZrO_2	3.0
As_2O_3	.5

A. SCANNING ELECTRON MICROSCOPY

The $[0°]_8$ SiC/CAS samples were mounted in Conductive Phenolic Mounting Compound (Konductomet I) using a spring tension clip to secure the sample in a fiber cross-section orientation. This cross-section provided ample coated and uncoated surfaces for analysis. The samples were initially polished with a rotating wheel mounted with silicon carbide grit paper with grits sizes of 320, 500, 1000, 2500 and 4000. The samples were then polished on a rotating wheel using 1.0 micron Buehler aerosol spray diamond compound. Scanning electron microscopy requires that samples be conductive consequently after polishing they were coated to a carbon thickness of 300 Å. The coating was applied using a No. 12560: EFFA MkII Carbon Coater.

Analysis of the microstructural and chemical compositions were verified using a Cambridge S200 SEM and a Kevex X-ray Energy Dispersive Spectrometer (EDS) with a light element detector. The Advanced X-ray Imaging process was performed on all samples to produce elemental maps to indicate elemental segregation within the matrix phases and the fibers. The Backscattered Secondary Electron (BSE) mode was utilized in producing micrographs to support experimental findings. This mode proved to be quite superior to the Secondary Electron (SE) mode in the identification of secondary phases developed during the hot corrosion process.

B. X-RAY DIFFRACTION

All samples were analyzed utilizing a Phillips XRG 3100 X-Ray Generator and a PW 1710 Diffractometer Controller. The data processing was performed using a Digital 3100 Vax Workstation. X-ray diffraction patterns were collected using an x-ray generator with a copper target ($K\alpha_1$ and $K\alpha_2$ wavelengths 1.54060 and 1.54439 Å) and a bent graphite crystal monochromator. The operating parameters were as follows: 30 Kv, 35 mA, angle range 10-90°and a scan rate of 5 seconds per every .02 degree increment.

Acquired data was processed by the Phillips APD 1700 software on a Vax workstation 3100. Spectral plots of intensity versus 2θ position were plotted for all samples received. The Phillips PW 1891 Total Access Diffraction Database (TADD) compared sample plots with library diffraction patterns at an extremely rapid rate. Several crystalline phases were detected and library intensity histogram diffraction patterns were plotted for comparison with spectral plots. The crystalline phases can be determined using the TADD in conjunction with JCPDS x-ray diffraction data cards.

V. RESULTS AND DISCUSSION

A. OPTICAL AND SCANNING ELECTRON MICROSCOPY (SEM)

Optical microscopy was performed on the as received SiC/CAS composite and a micrograph (Figure 13) was produced showing the $[0°]_8$ fiber orientation within the matrix. The sample shows an even spatial distribution of fibers with small areas of matrix concentrated regions.

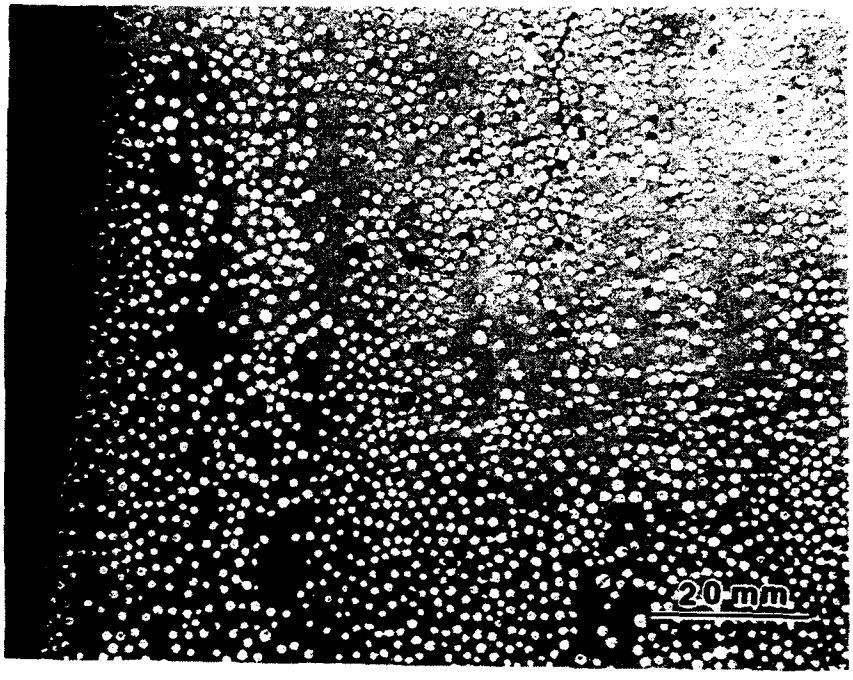

Figure 13. SiC/CAS As-Received Optical Micrograph at x75 Magnification

Scanning electron microscopy was performed on all samples provided by NAWC. The as received sample was analysed using the SEM and a back scattered micrograph depicting surface morphology is presented in Figure 14. Advanced x-ray imaging of the composite is presented in Figure 15. indicating concentrations of Ca, Al and Si. The CAS matrix appeared to be dominantly single phase anorthite ($CaAl_2Si_2O_8$), based on the composition provided by NAWC in Table I and by plotting the composition on the $CaO \cdot Al_2O_3 \cdot SiO_2$ ternary phase diagram (Figure 2).

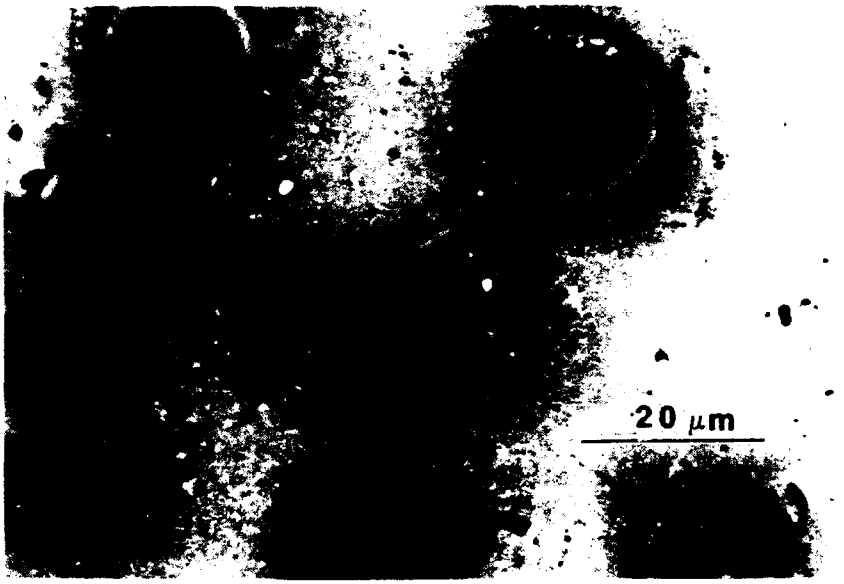

Figure 14. BSE Micrograph of As-Received SiC/CAS

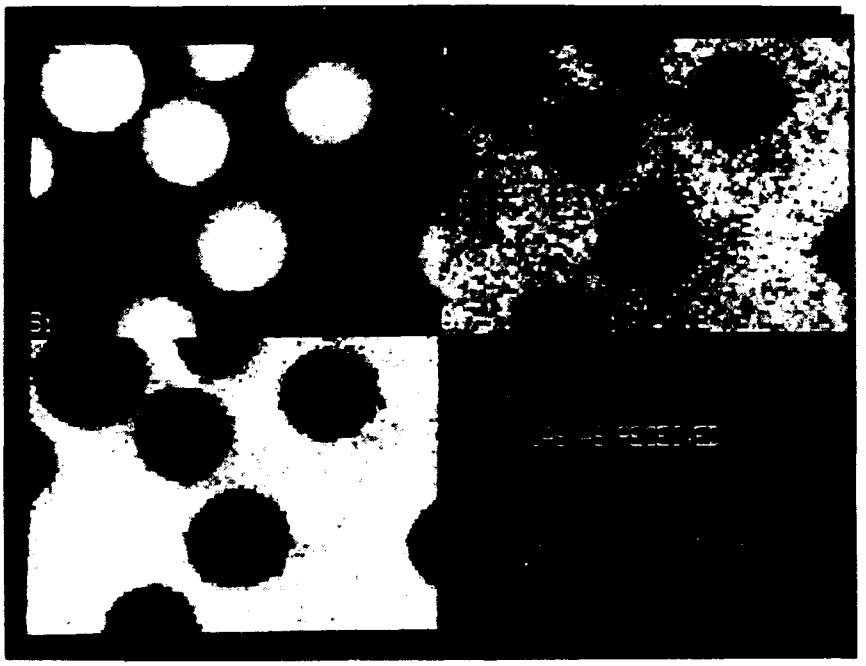

Figure 15. Advanced X-Ray Image of Figure 14

EDX analysis was performed on the CAS matrix and the composition is presented in Table III.

TABLE III. SiC/CAS EXPERIMENTAL MATRIX COMPOSITION [Ref. 16]

OXIDE COMPONENTS	COMPOSITION (WT%) NAWC	COMPOSITION (WT%) EXPERIMENTAL
CaO	18.5	34.8
Al_2O_3	38.5	28.6
SiO_2	39.5	34.0
ZrO_2	3.0	2.1
As_2O_3	0.5	0.5

This analysis has shown a difference between the as received CAS composition (provided by NAWC) and that resulting from the experiment. The EDX (Figure 16) analysis indicates a significant increase in the calcium oxide content and a subsequent decrease in the aluminum and silicon oxides. The difference in the calcium oxide composition may be attributed to a glassy phase within the anorthite matrix or possible calcium oxide segregation resulting from a non-homogeneous matrix batching process.

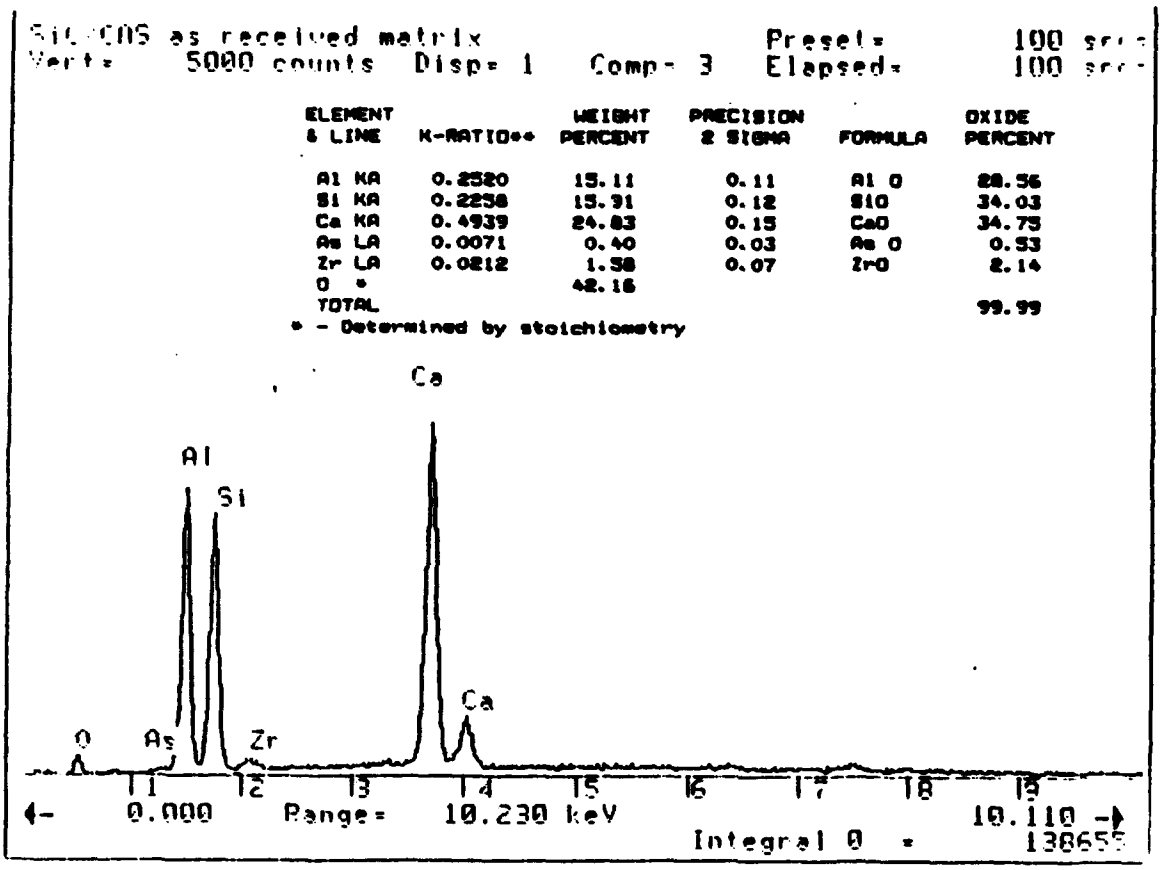

Figure 16. EDX Analysis of As-Received CAS Matrix

Small bright particles (up to 5μm in diameter), evenly dispersed throughout the matrix, were determined to be zircon ($ZrO_2 \cdot SiO_2$) as verified by SEM analysis. EDX spectrum analysis (Figure 17) yielded a 1:1 zirconium oxide to silicon oxide atomic percent ratio. Small particles (< 1 μm), believed to be zircon (or zirconia), were also present on grain boundaries. Grain sizes were observed to be as large as 6 μm in diameter. A micrograph of a large zircon particle is

presented in Figure 18. X-ray elemental mapping (Figure 19) indicates the zircon particle contains concentrated regions of Zr and Si.

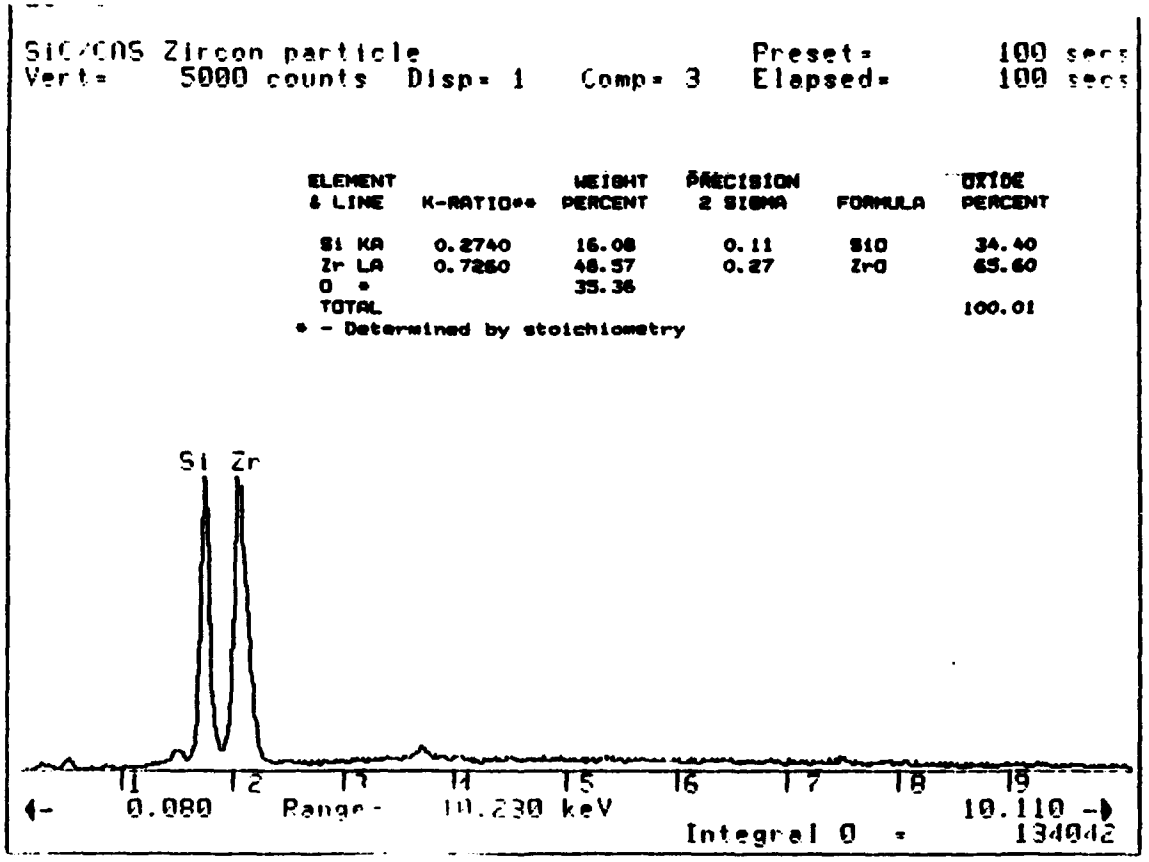

Figure 17. EDX Analysis of Zircon Particle in As-Received SiC/CAS

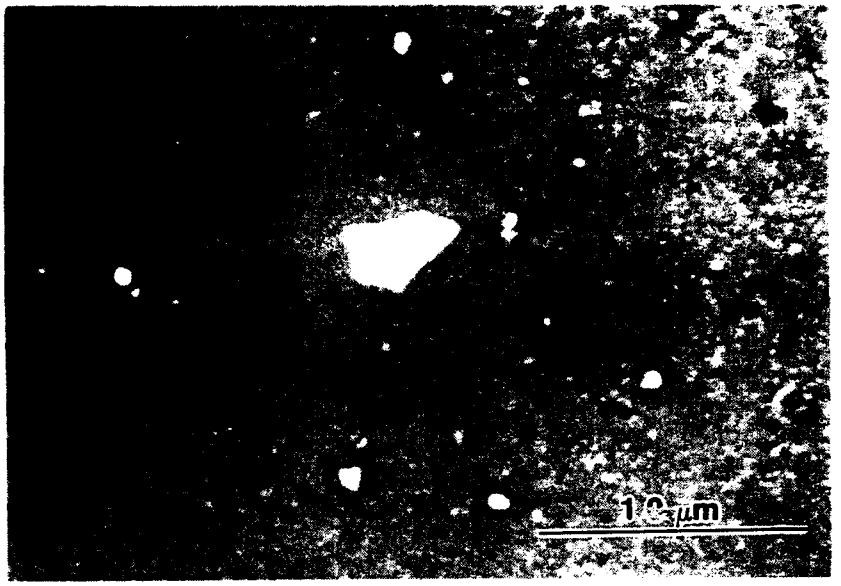

Figure 18. BSE Micrograph of Zircon Particle in As-Received Sample

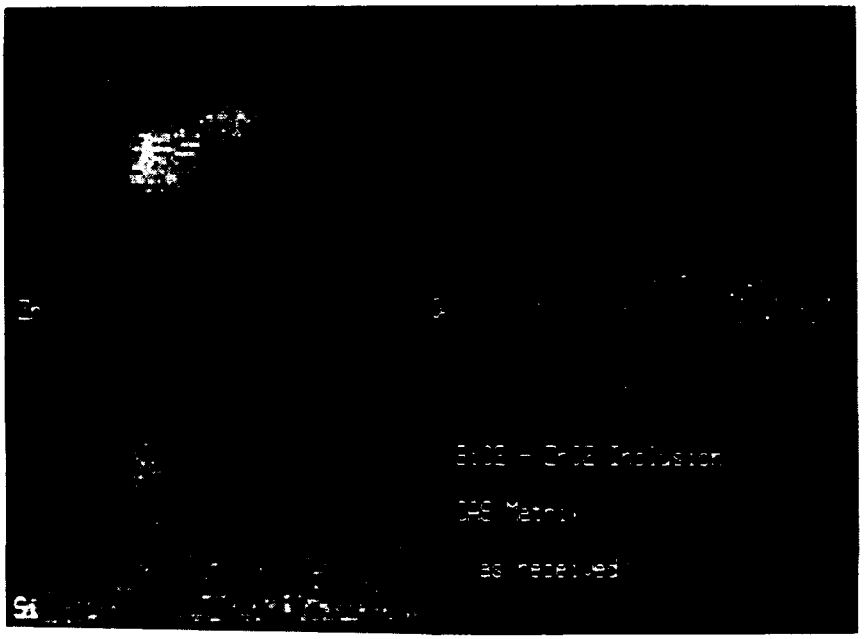

Figure 19. X-ray Elemental Micrograph of Zircon Particle Shown Above

Scanning electron microscopy performed on the Na_2SO_4 coated SiC/CAS composite heat treated in air to 900 °C revealed corrosion along the entire surface of the composite. The extent of the corrosion is controlled by the rate of oxygen diffusion into the composite which results in the degradation of the SiC-fiber and glass-ceramic matrix. Oxygen diffusion may be enhanced by the presence of matrix cracking which acts as a transport mechanism for corrosion products to the inner matrix and reinforcing fiber regions. The corrosive reaction zone was approximately 20-50 μm deep into the composite (Figure 20).

Figure 20. BSE Micrograph of Na_2SO_4 Coated SiC/CAS Composite Heat Treated in Air at 900° C

Significant matrix/fiber attack is evident in the coated sample (Figure 20) as compared to the lack of degradation of the composite in the uncoated sample (Figure 21).

Figure 21. BSE Micrograph of Uncoated SiC/CAS Composite Heat Treated in Air to 900 °C

Within the reaction layer it is apparent that the matrix has reacted with the corrosion products and has created numerous new crystalline and most probably amorphous phases. In addition, near the surface, complete fiber degradation has occurred to a depth of approximately 15 µm. Degradation of fibers also appeared to have lead to reactions producing new phases.

These new crystalline and amorphous phases have formed as a result of the hot corrosive effects of the sodium sulfate salt. EDX analysis of the crystalline phases (Figure 22 and

Figure 23) showed a stoichiometric relationship for two calcium silicate phases, wollastonite (1:1 Ca to Si) and rankinite (3:2 Ca to Si). Additionally an amorphous two phase region believed to be a silicon rich glassy phase and some other crystalline phases had formed which could not be resolved due to the limit of resolution of the SEM. The use of quarternary phase diagrams along with EDX analysis failed to identify stoichiometric phases present in this glassy region.

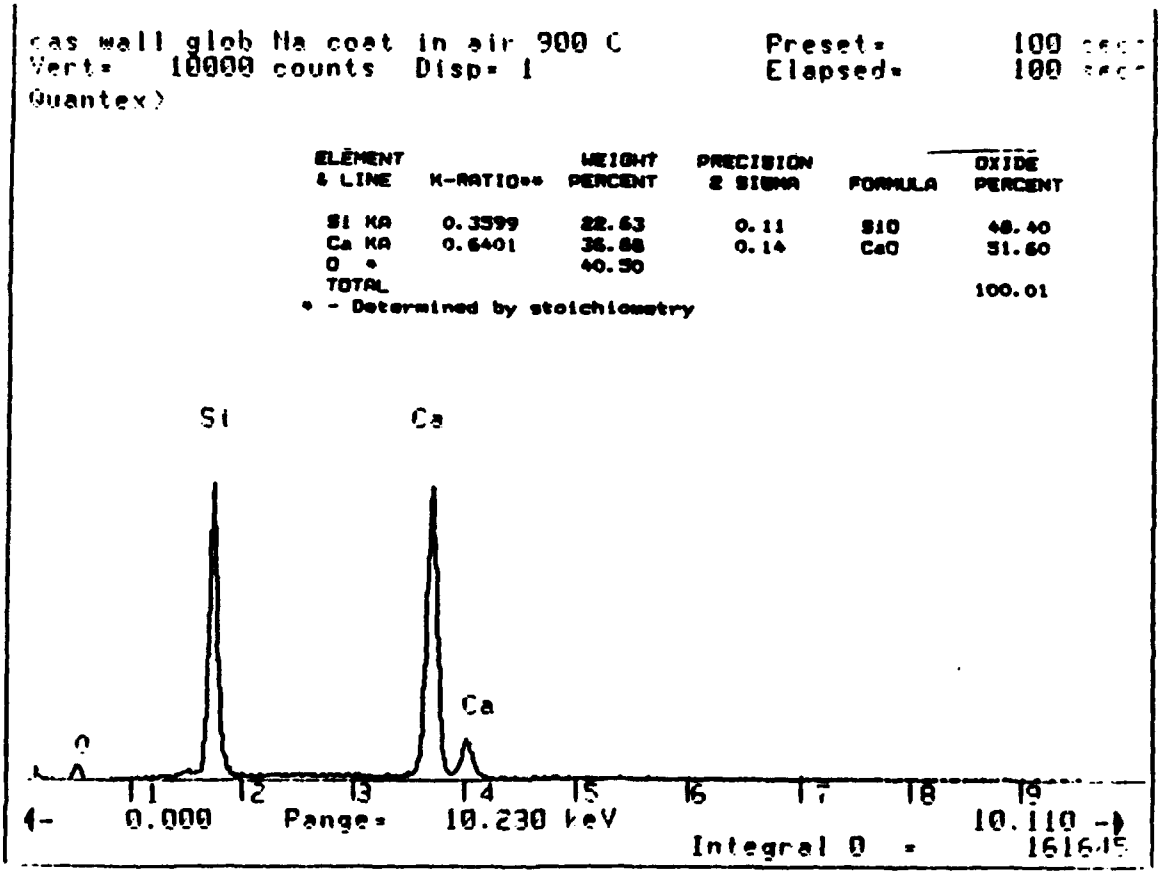

Figure 22. EDX Analysis Na_2SO_4 Coated Heat Treated in Air at 900 °C, Wollastonite Phase

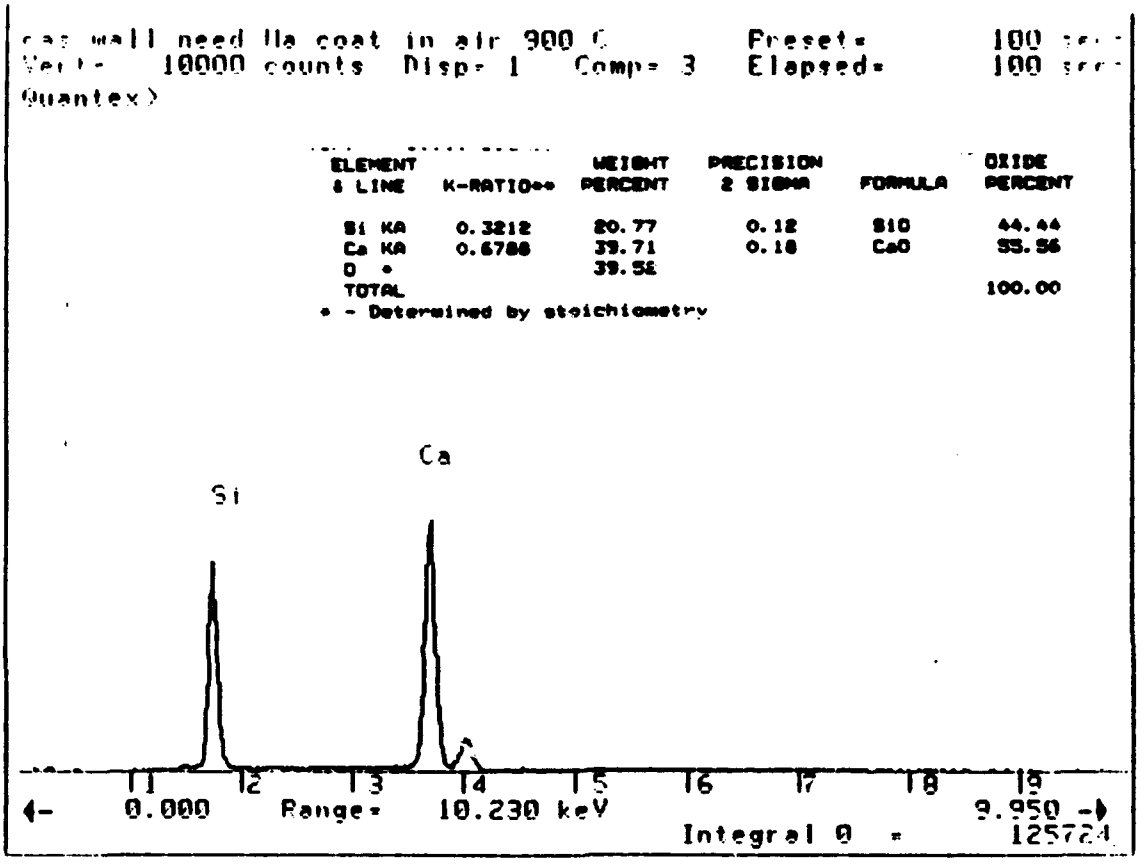

Figure 23. EDX Analysis Na_2SO_4 Coated Heat Treated in Air at 900 °C, Rankinite Phase

The wollastonite morphology is represented as globular bright phases in Figure 20. The rankinite forms as needle like phases as in Figure 24. Advanced x-ray imaging indicates high calcium concentration in the needle like structure (Figure 25).

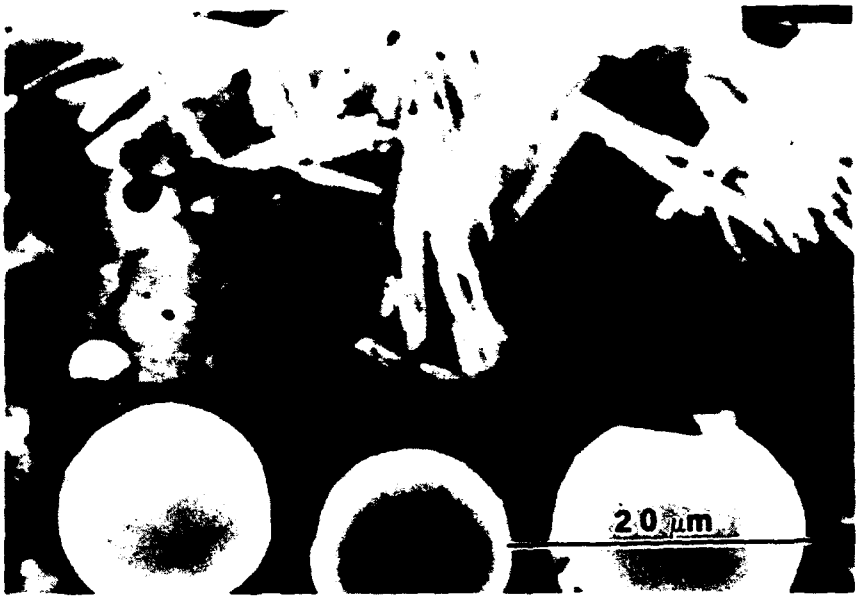

Figure 24. BSE Micrograph of Rankinite

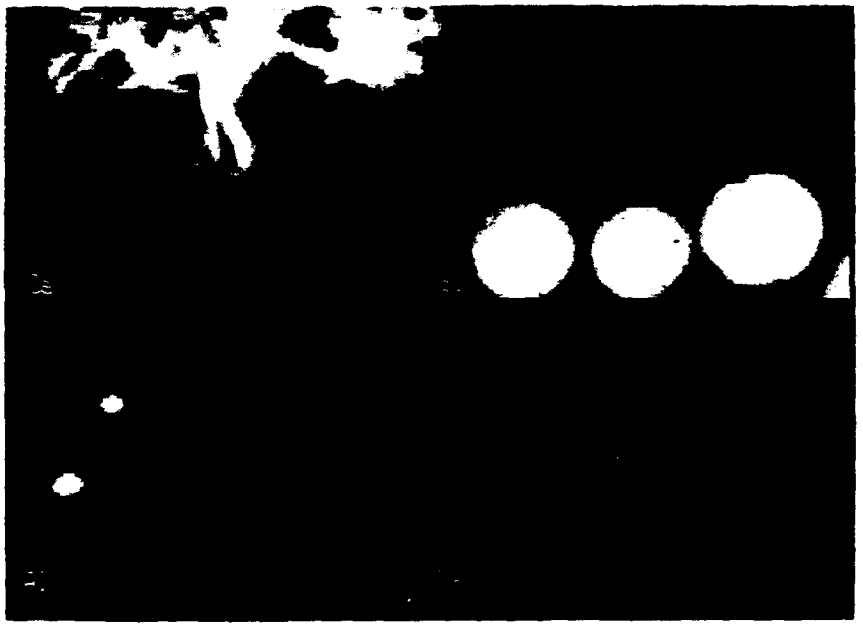

Figure 25. Advanced X-Ray Image of Rankinite Shown in Figure 24

The two phase glassy regions, shown in Figure 20, are characterized by a dark grey phase near the surface and a lighter grey phase near the middle of the reaction zone. EDX analysis was performed on the light grey region and is presented in Figure 26. This region is believed to

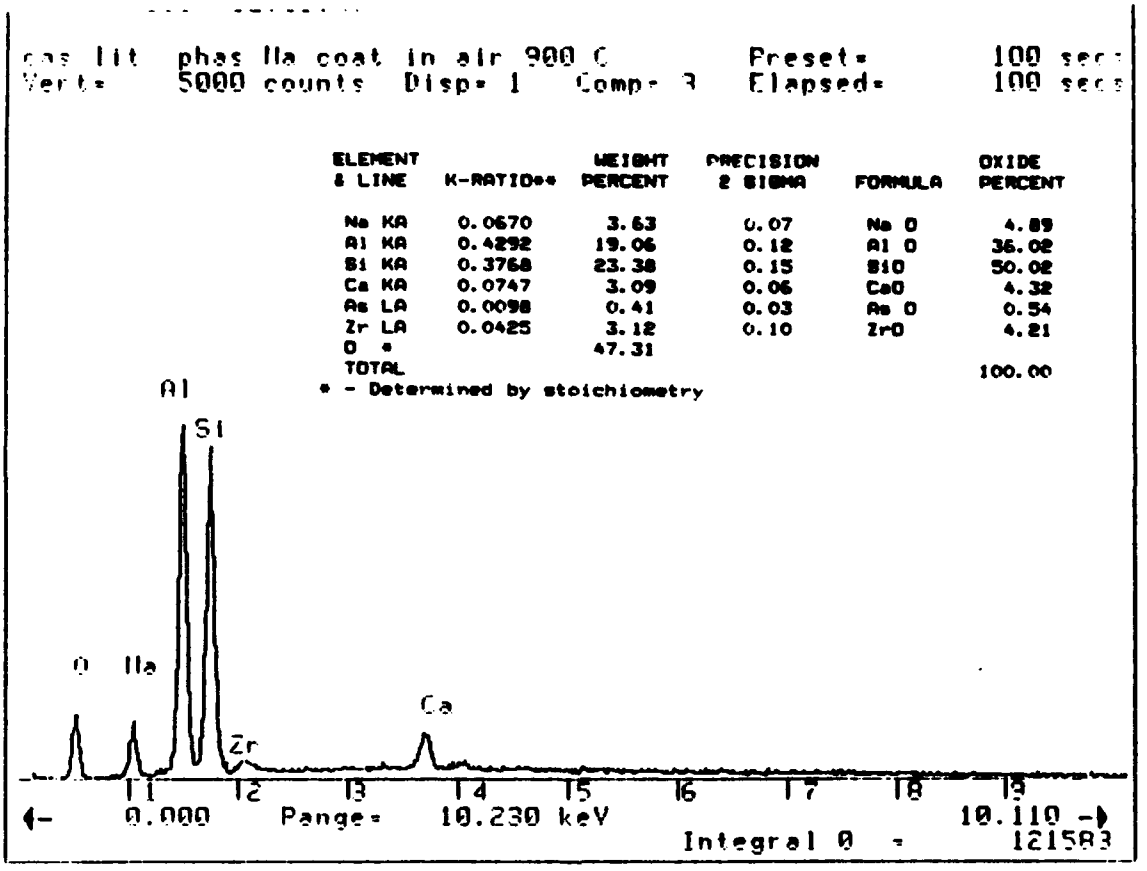

Figure 26. EDX Analysis Na_2SO_4 Coated Heat Treated in Air at 900° C for 100 Hours

consist of a glassy phase and other crystalline phases. This analysis was unable to provide stoichiometric results for phase resolution.

EDX analysis (Figure 27) was performed on the dark grey phase that forms at the surface (Figure 20). This analysis indicates a dominently high concentration of silicon. This dark phase also forms as a silicon rich ring around fibers as they degrade (Figure 28.) Advanced x-ray analysis of this ring (Figure 29) indicates a silicon rich region surrounding the degraded fiber.

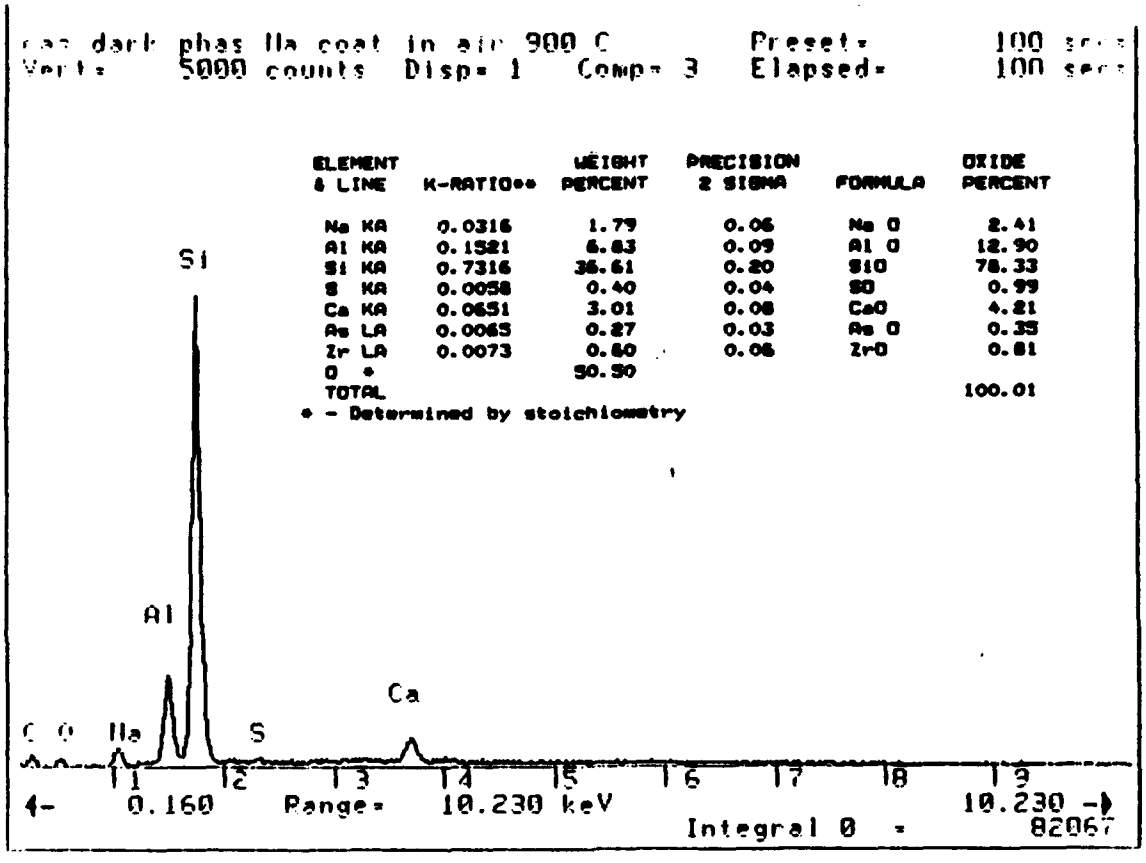

Figure 27. EDX of Dark Phase Region Coated in Air at 900°C

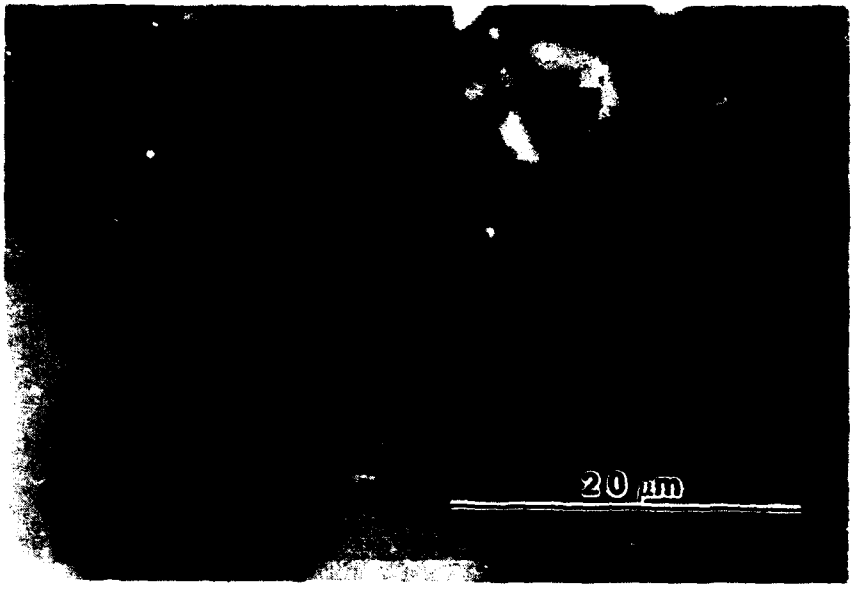

Figure 28. BSE Micrograph Indicating Silicon Rich Region in $Na2SO_4$ Coated SiC/CAS Heat Treated in Air at 900°C

Figure 29. Advanced X-ray Image of Silicon Rich Region Shown in Figure 28

The optical and scanning electron microscopy has indicated that the protective SiO_2 layer is believed to be completely destroyed by the corrosive effects of the Na_2SO_4 coating and subsequently fiber attack occurs until the fiber is completely degraded.

The salt coated sample heat treated in argon to 900 °C is shown in Figure 30.

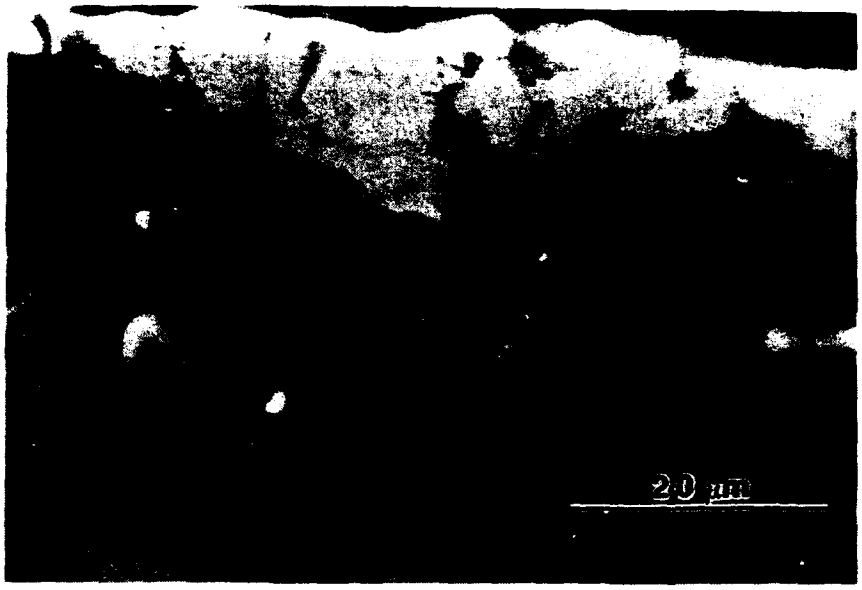

Figure 30. BSE Micrograph of Na_2SO_4 Coated SiC/CAS Heat Treated in Argon to 900° C

Fiber degradation is less severe than in the sample heat treated in air. The reaction zone was approximately 20-30 µm deep and extends over the length of the composite. The only fibers that were attacked by the Na_2SO_4 salt were those located at the surface. The uncoated side of the sample shows little if no fiber/matrix degradation (Figure 31) which was as expected since limited corrosion occurred at the surface of the uncoated sample heat treated in air (Figure 21).

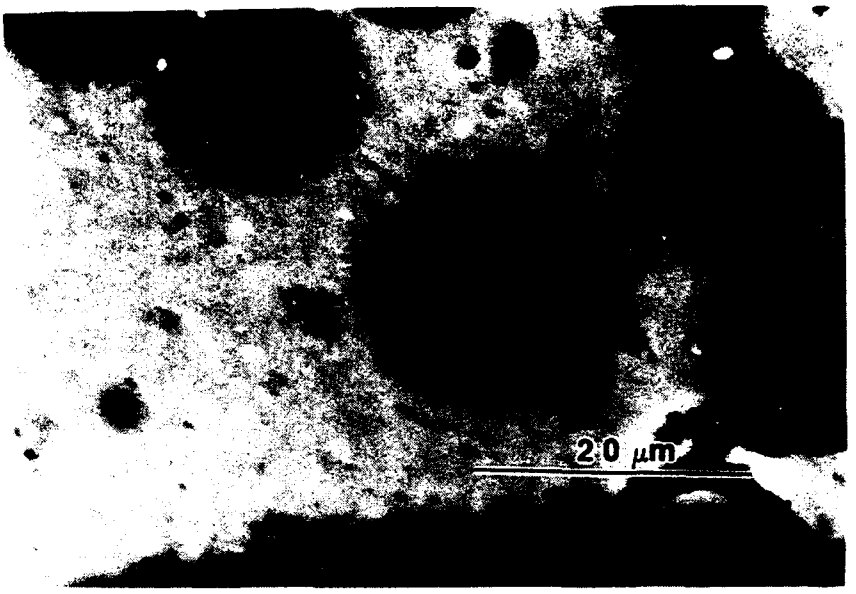

Figure 31. BSE Micrograph of Uncoated Side of SiC/CAS in Argon Heat Treated to 900° C

The crystalline phases that formed in argon were very similar to those in air. The rankinite crystalline phase had again formed, as verified in Figure 23, however much less of this needle like structure was present. EDX analysis (Figure 22) indicated the presence of the globular wollastonite phase and is shown in Figure 32. In this micrograph it is noted that the wollastonite has formed in the regions previously occupied by the fiber. Advanced x-ray imaging indicates Ca, Si, O and Na rich regions occuring in the reaction zone (Figure 33).

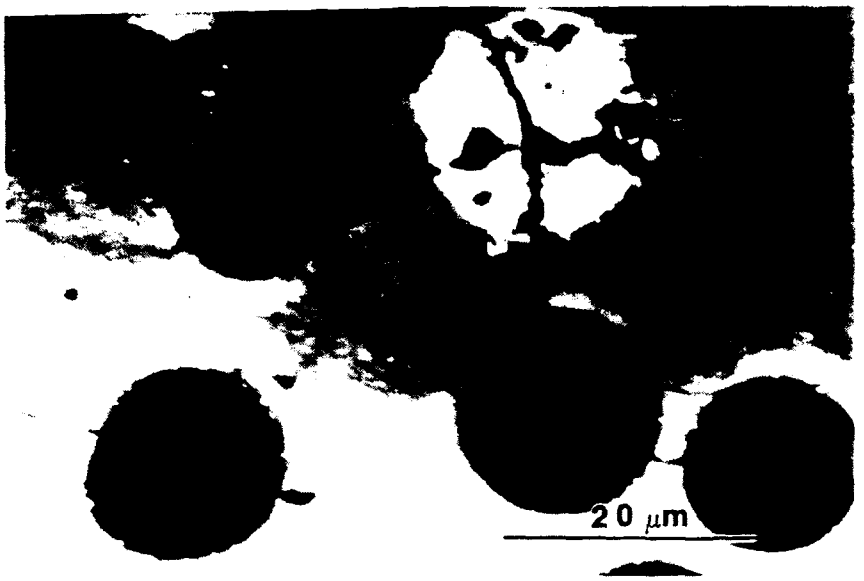

Figure 32. BSE Micrograph of SiC Fiber Degradation in Coated SiC/CAS Heat Treated in Argon to 900° C

Figure 33. Advanced X-Ray Imaging of Reaction Zone in Coated SiC/CAS Heat Treated in Argon at 900° C (Shown in Figure 32)

The amorphous glassy phases that have formed in argon were very similar to those formed in air. The two phase region (light and dark grey) is shown in Figure 30. EDX analysis has shown similar data for the light grey phase (Figure 26). EDX analysis (Figure 34) has shown that the dark grey silicon rich glassy phase contains small amounts of Sulfur which were not present in the sample exposed in air.

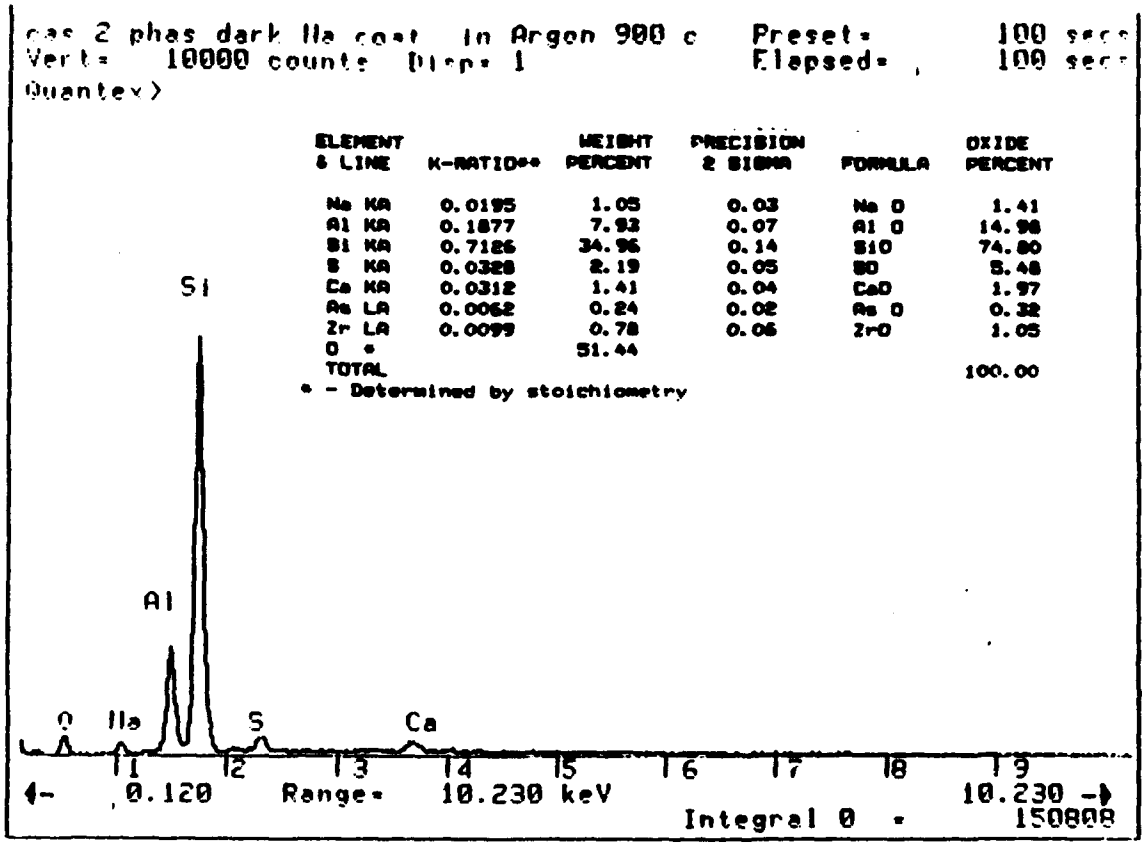

Figure 34. EDX of Coated SiC/CAS Heat Treated in Argon at 900° C

One noteworthy observation is the mechanism of corrosive attack along matrix cracks (Figure 35). Corrosive phases have formed, on the order of 1 μm, on the crack interface and EDX analysis was unable to identify these phases due to the large limit of resolution of the SEM in the EDX mode. When comparing reaction phase morphology it is believed the bright

phases are pseudo-wollastonite and the dark regions are silicon rich glassy phases.

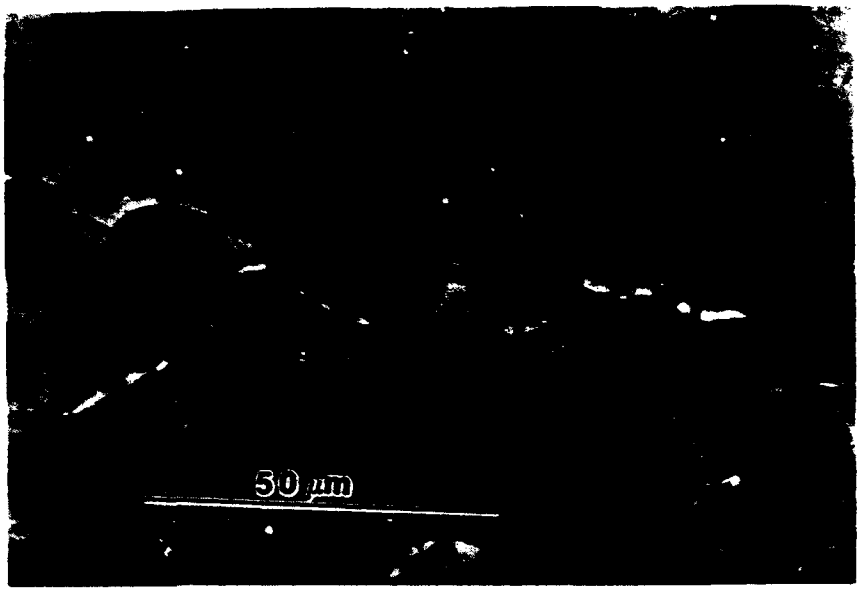

Figure 35. BSE Micrograph of Corrosion Along Matrix Cracking in Coated Sample Heat Treated in Argon to 900° C

Optical and scanning electron microscopy have shown substanti matrix corrosion to a depth of 20 μm with significantly less fiber degradation (fibers intact at 10 μm from surface) occurring in an argon atmosphere.

B. X-RAY DIFFRACTION (XRD) ANALYSIS

X-ray diffraction analysis was conducted on the as-received and heat treated/coated samples. This determined the baseline crystalline structure of the SiC/CAS composite and the resulting post heat treatment phases present. The XRD pattern for the as-received sample is presented in Figure 36. Crystalline phases and their respective Miller indices were determined for each intensity peak utilizing a VAX 3100 workstation in conjunction with the Phillips APD 1700 software package. The software data included d-spacings, peak intensities and 2θ positions for each intensity peak in the diffraction pattern. This information was then used to verify the correct Miller indices (for each phases present) utilizing the Hanawalt JCPDS diffraction pattern cards.

In the as-received sample the main crystalline phase was determined to be anorthite. This confirmed the composition provided by NAWC as presented in Table I. Other phases present were β-SiC and zircon. These phases were verified by XRD pattern analysis and are presented in Figure 37. The anorthite and zircon phases are matrix constituents and the β-SiC phase is present in the fiber.

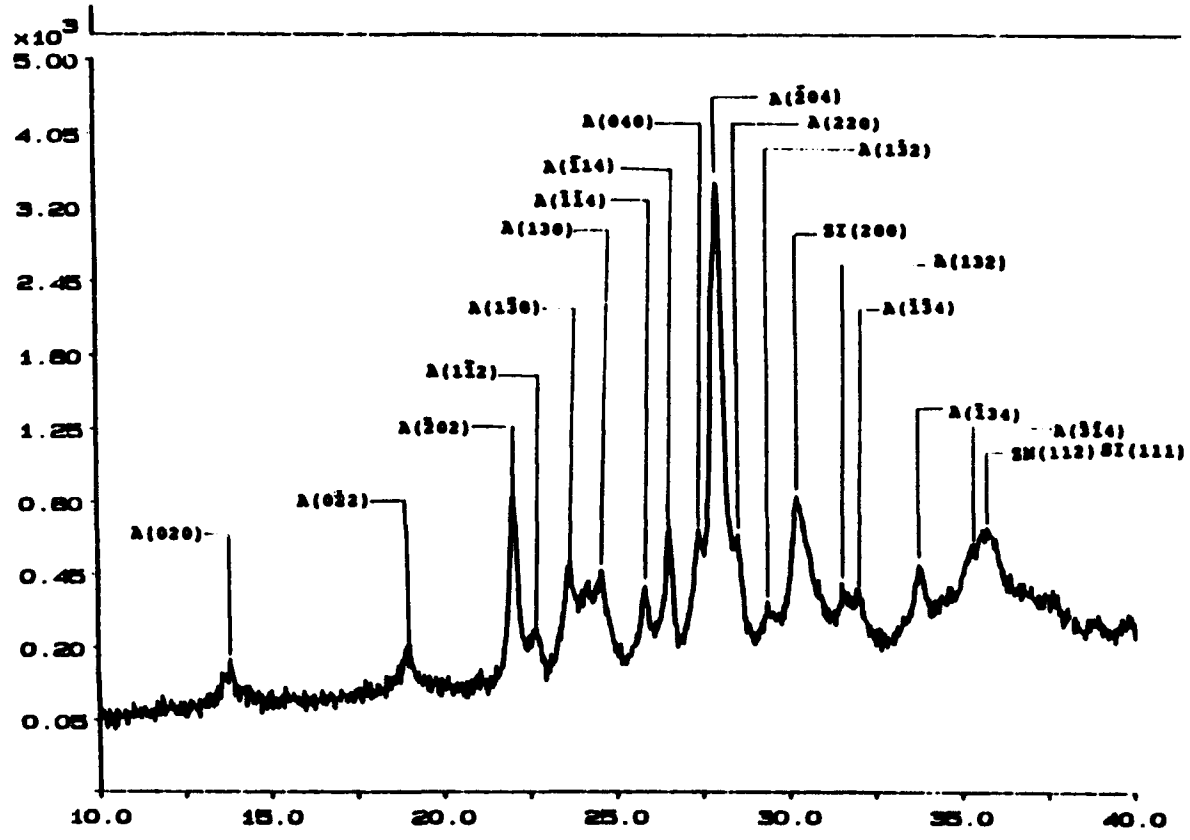

Figure 36. X-ray Diffraction Patterns of As-Received SiC/CAS Specimen Showing Crystalline Phases and Miller Indices. A = Anorthite, ZI = Zircon, SI = β-SiC

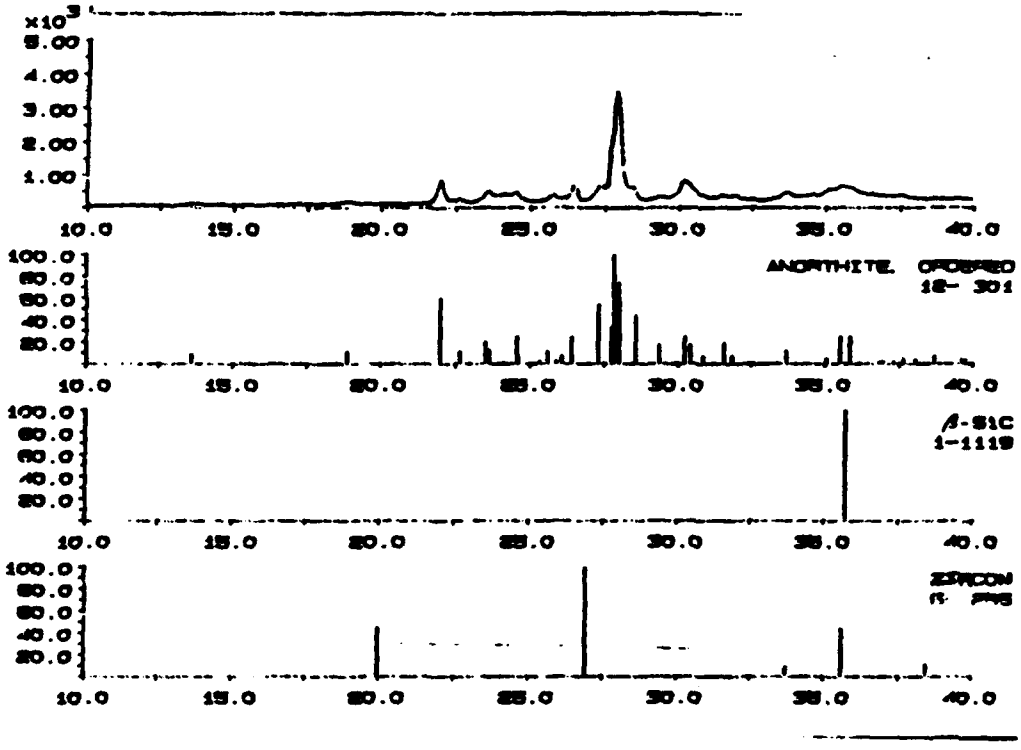

Figure 37. XRD Pattern for As-Received SiC/CAS Sample

The major phases and their respective relative intensities, Miller indices and 2θ positions are presented in Table IV.

TABLE IV. PHASES PRESENT, RELATIVE INTENSITIES, MILLER INDICES AND LINE POSITIONS (2θ) IN THE AS-RECEIVED SPECIMEN.

PHASES	RELATIVE INTENSITIES	MILLER INDICES (HKL)	2θ (DEGREES)
ANORTHITE (TRICLINIC)	100	(204)	27.8
	60	(202)	22.0
	33	(040)	27.3
ZIRCONIA (TETRAGONAL)	100	(200)	30.1
ZIRCON (TETRAGONAL)	44	(112)	35.6
β-SiC (CUBIC)	100	(111)	35.8

The as-received XRD pattern is compared to that of the salt coated and heat treated in air and argon samples in Figure 38. It is evident that the main anorthite peak (27.8°) is significantly reduced as the matrix reacts with the corrosive environment. Additionally the β-SiC peak (35.8°) is

decreased as the fiber reacts with corrosive products. Numerous new crystalline phases are formed as can be seen by the presence of new XRD intensity peaks. Also noteworthy is evidence of glassy phases as seen by the increase of the background in the XRD patterns of the reacted samples.

In the sodium sulfate coated sample heat treated in air the new phases formed were albite, nepheline, wollastonite and rankinite. The anorthite matrix that was unaffected (outside reaction zone) was still detected as well as the β-SiC and zircon phases. The XRD pattern is provided in Figure 39. The Miller indices were determined for each phase and are presented in Figure 40. This crystallographic data is in excellent agreement with the SEM/EDX data although it still does not allow us to resolve between the glassy and crystalline regions other than for wollastonite and rankinite which are clearly defined.

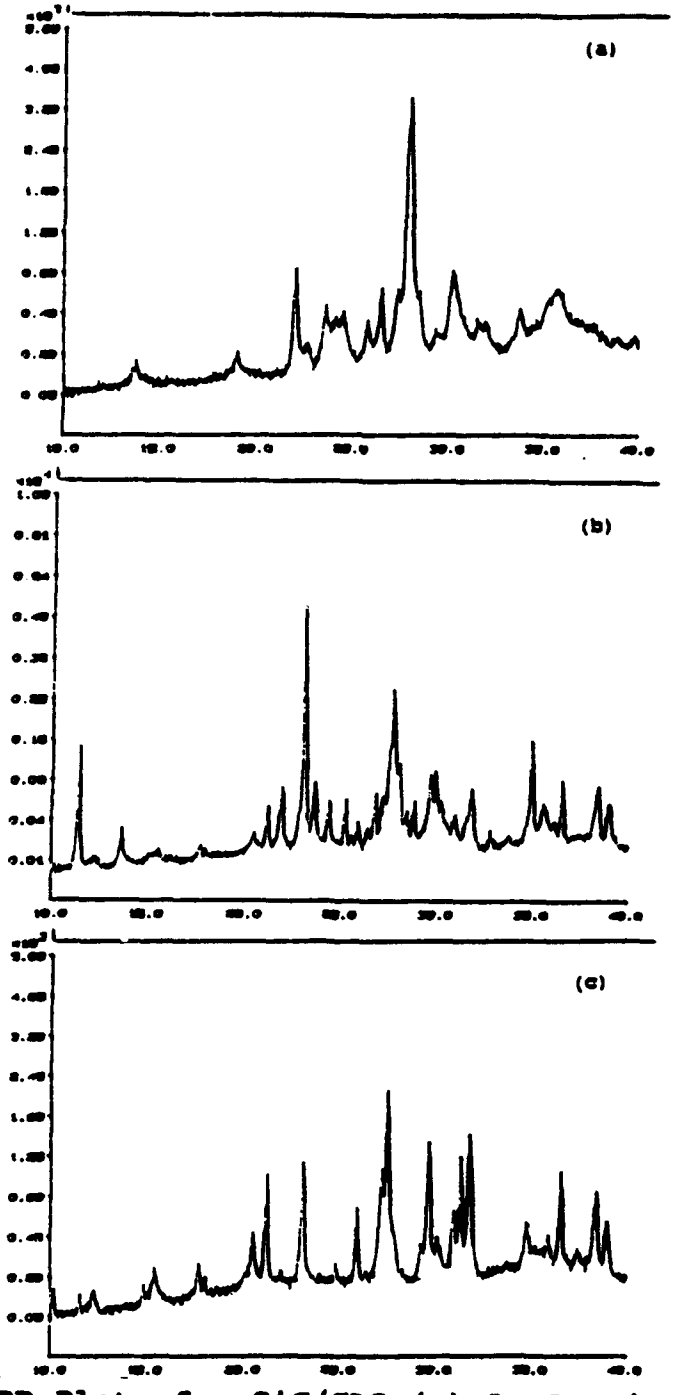

Figure 38. XRD Plots for SiC/CAS (a) As-Received, (b) Salt Coated in Air at 900° C, (c) Salt Coated in Argon at 900° C

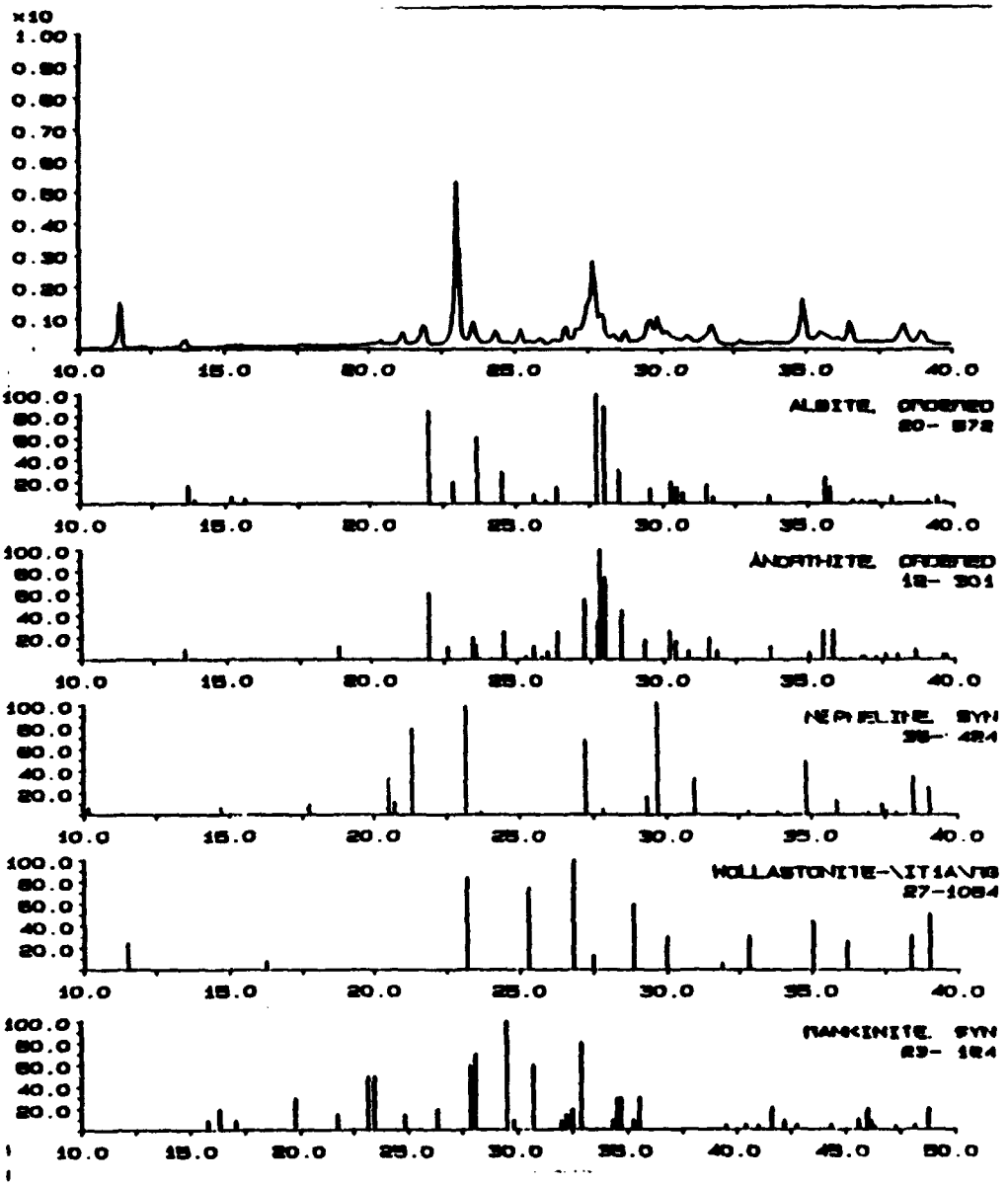

Figure 39. XRD Pattern for Salt Coated SiC/CAS Reacted in Air at 900° C

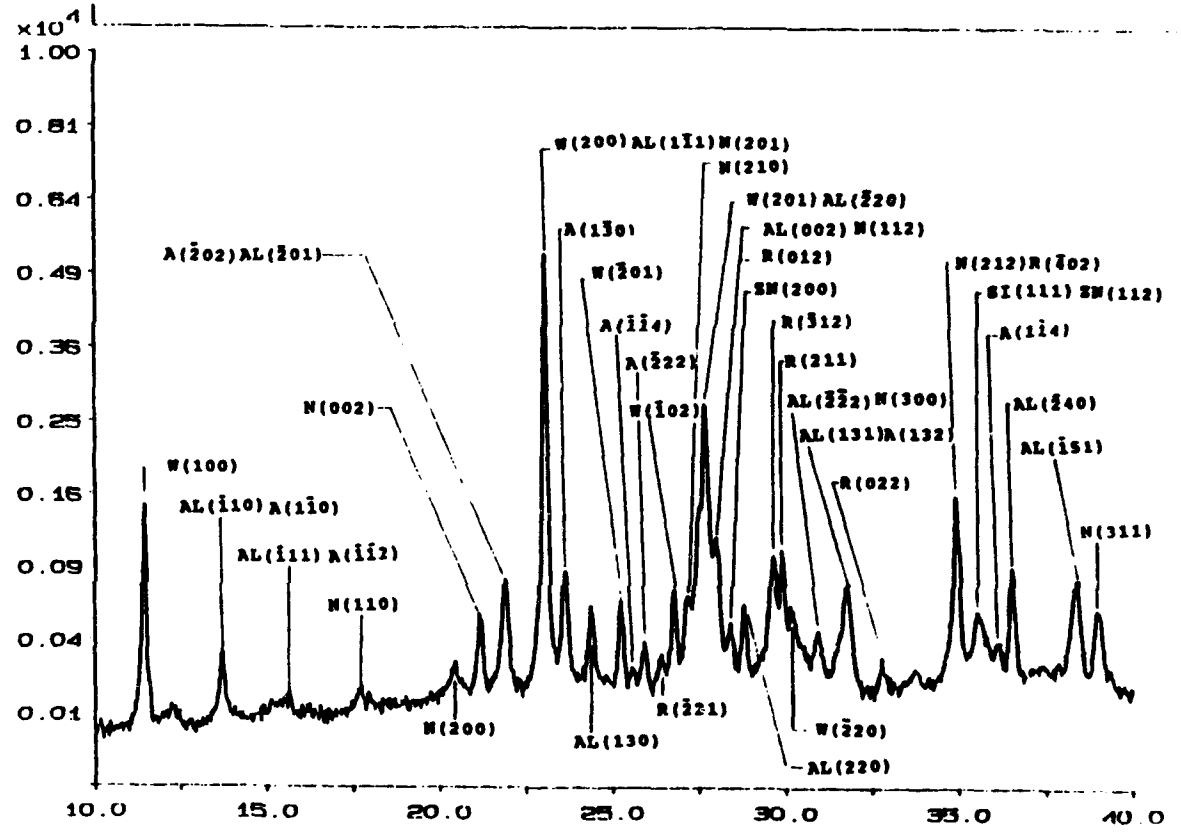

Figure 40. X-ray Diffraction Patterns of SiC/CAS and Reacted in Air at 900° C Showing Crystalline Phases and Miller Indices. A = Anorthite, W = Wollastonite, AL = Albite, N= Nepheline, SI = β-SiC, ZN = Zirconia, R = Rankinite

Table V shows the major phases present with their respective relative intensities, Miller indices, and 2θ positions.

TABLE V. PHASES PRESENT, RELATIVE INTENSITIES, MILLER INDICES AND LINE POSITIONS (2θ) IN COATED SAMPLE HEAT TREATED IN AIR

PHASES	RELATIVE INTENSITIES	MILLER INDICIES (HKL)	2θ (DEGREES)
ALBITE (TRICLINIC)	100	(220)	27.7
	88	(201)	21.9
	88	(002)	28.0
ANORTHITE (TRICLINIC)	60	($\bar{2}$02)	21.9
	26	(1$\bar{1}$4)	35.5
	20	(1$\bar{3}$0)	23.6
NEPHELINE (HEXAGONAL)	100	(201)	23.1
	80	(002)	21.2
	70	(210)	27.1
WOLLASTONITE (TRICLINIC)	100	($\bar{1}$02)	26.8
	85	(200)	23.1
	73	($\bar{2}$01)	25.2
RANKINITE (MONOCLINIC)	100	($\bar{3}$12)	29.6
	79	(022)	32.8
	60	(012)	27.7
ZIRCON (TETRAGONAL)	100	(200)	26.9
	42	(112)	35.6
β-SiC (CUBIC)	100	(111)	35.8

In the sodium sulfate coated sample heat treated in argon at 900° C, similar phases have formed despite being in an oxygen deficient atmosphere. An oxygen deficient chemical reaction occurs and leads to the formation of mullite and pseudo-wollastonite (a high temperature low pressure form of wollastonite) crystalline phases. The common phases to the sample exposed to salt in air are anorthite, rankinite, albite and nepheline. The XRD pattern for this specimen is shown in Figure 41. The Miller indices were determined and are presented in Figure 42.

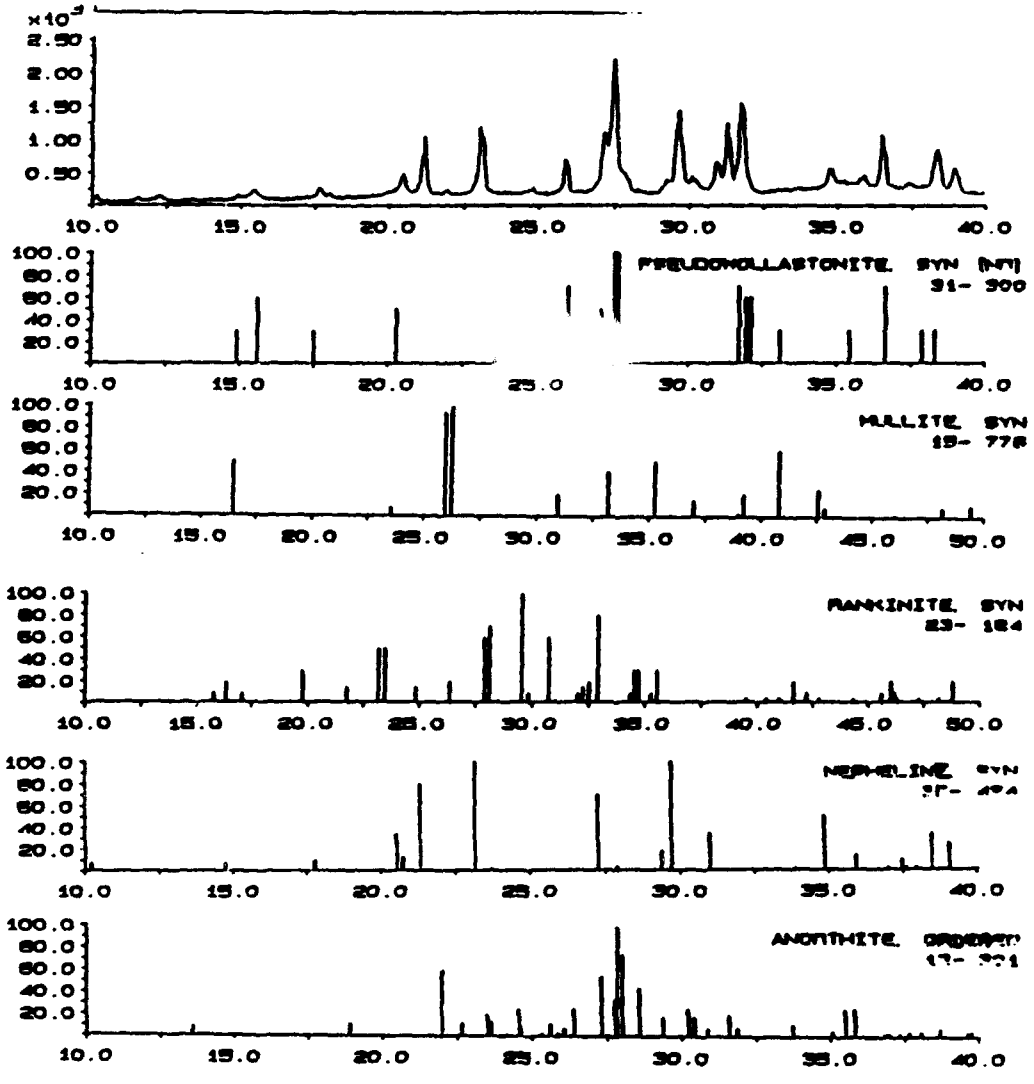

Figure 41. XRD Pattern for Salt Coated SiC/CAS Sample Reacted in Argon at 900° C

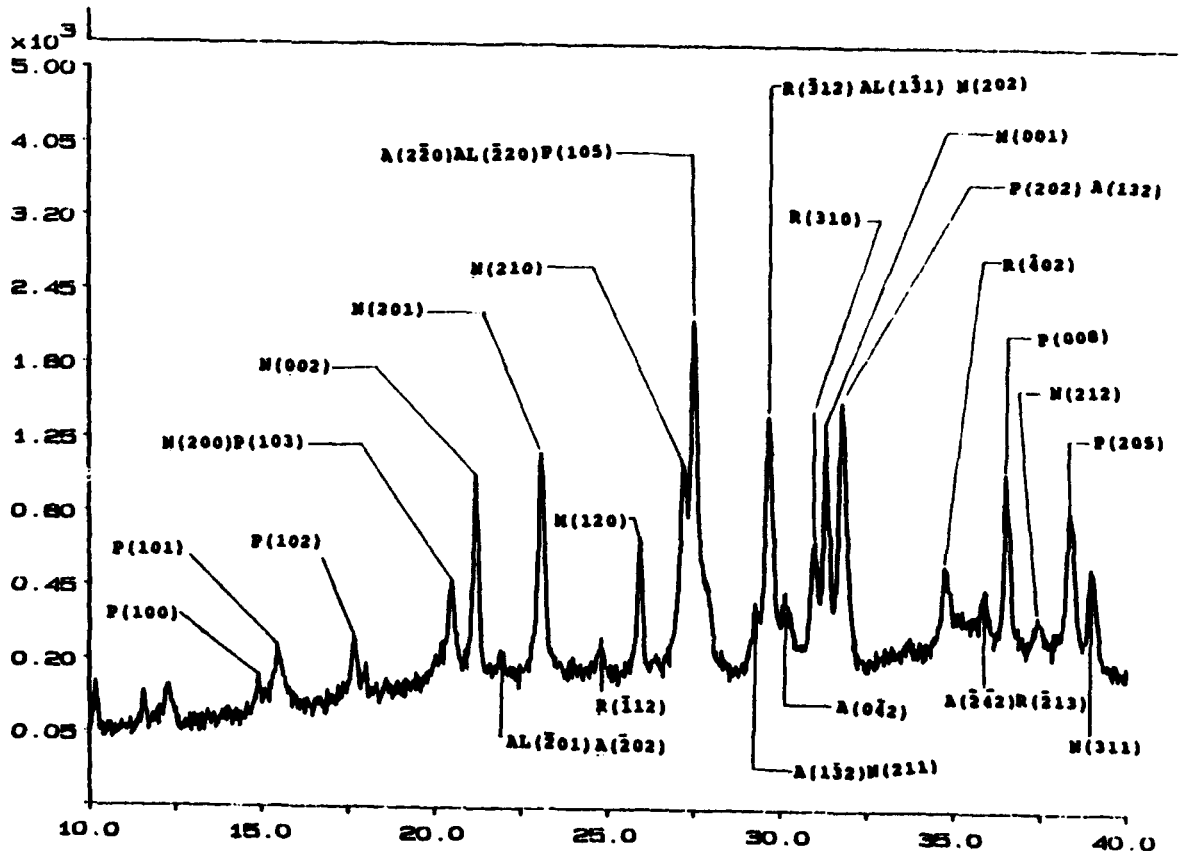

Figure 42. X-ray Diffraction Pattern of SiC/CAS Salt Coated and Reacted in Argon at 900° C Showing Crystalline Phases and Miller Indices. P = Pseudo-Wollastonite, N = Nephelline, A = Anorthite, AL =Albite, R = Rankinite

Table VI indicates major phases present with their respective relative intensities, Miller indices and 2θ position.

TABLE VI. PHASES PRESENT, RELATIVE INTENSITIES, MILLER INDICES AND LINE POSITIONS (2θ) IN SALT COATED SAMPLE HEAT TREATED IN ARGON AT 900° C.

PHASES	RELATIVE INTENSITIES	MILLER INDICIES (HKL)	2θ (DEGREES)
ALBITE (TRICLINIC)	100	$(\bar{2}20)$	27.5
	85	$(\bar{2}01)$	22.3
	14	$(1\bar{3}1)$	29.7
ANORTHITE (TRICLINIC)	60	$(\bar{2}02)$	21.9
	55	$(2\bar{2}0)$	27.2
	25	$(0\bar{4}2)$	30.2
NEPHELINE (HEXAGONAL)	100	(201)	23.1
	100	(202)	29.7
	80	(002)	21.2
PSEUDO WOLLASTONITE (TRICLINIC)	100	(105)	27.5
	70	(202)	31.8
	70	(008)	36.5
RANKINITE (MONOCLINIC)	100	$(\bar{3}12)$	29.7
	60	(310)	30.9
	30	$(\bar{4}02)$	34.8
MULLITE (ORTHORHOMBIC)	95	(120)	25.9
	19	(001)	31.3

In the comparison of XRD and SEM results it is seen that the major hinderance in the phase identification process is the existence of glassy phases which are formed by the manufacturing process and subsequent heat treatment. Although only the calcium silicate phases of wollastonite, rankinite and pseudo-wollastonite were able to be resolved by the SEM, there is an overwhelming presence of albite, anorthite, nepheline and mullite phases detected by XRD analysis which appear to be associated with glassy phases. The limit of resolution of the SEM in the backscattered mode and the EDX mode produced a complete analysis of those regions which were not some form of calcium silicate.

C. CHEMICAL REACTIONS

The following section will suggest some chemical reactions to show how the numerous phases could have possibly formed in the corroded SiC/CAS composite. It has been suggested by Kowalik, Wang and Sands that the fibers initially oxidize in air by the following reactions:

$$SiC_{(s)} + 1.5\ O_{2\ (g)} = SiO_{2\ (s)} + CO_{(g)}$$

The sodium sulfate oxide forms by the following equation:

$$Na_2SO_4 = Na_2O_{(l)} + SO_{3\ (g)}$$

The nepheline and wollastonite form by the following equations:

$$Na_2SO_4 + CaAl_2Si_2O_8 + SiO_2 = 2NaAlSiO_4 + CaSiO_3 + SO_3$$

The gas produced by these reactions evolves out of the matrix leaving some gas porosity. [Ref. 2: pg. 5]

The remaining phases of albite and rankinite are possibly formed by the following reactions:

$$Na_2O + 4\ SiO_2 + CaAl_2Si_2O_8 = 2\ NaAlSi_3O_8 + CaO$$

$$3\ CaO + 2\ SiO_2 = Ca_3Si_2O_7$$

The development of the possible chemical reaction for sample that has reacted in argon is quite different as there is a lack of oxygen diffusion into the matrix to drive the corrosion process. Kowalik, Wang and Sands have indicated that the sodium sulfate salt is believed to form sodium oxide by the following equation:

$$Na_2SO_4 = Na_2O_{(l)} + SO_2 + 1/2\ O_2\ (g)$$

Once again the gas bubbles evolve from the matrix leaving residual porosity. [Ref. 2: pg. 5]

The remaining phases of nepheline, albite, mullite, pseudo-wollastonite and rankinite are possibly formed by the

following reactions:

$$Na_2SO_4 + 4\ CaAl_2Si_2O_8 = NaAlSiO_4 + NaAlSi_3O_8 + Al_6Si_2O_{13} + 4\ CaO + 2\ SiO_2 + SO + O_2$$

$$4\ CaO + 3\ SiO_2 = Ca_3Si_2O_7 + \alpha - CaSiO_3$$

The only phases that could be identified as stoichiometric by EDX analysis were the calcium silicate phases. All other phases were contained in what is believed to be an amorphous mixture of glassy and crystalline phases that lie in the reaction zones of the samples that were coated and reacted in air and argon.

VI. CONCLUSIONS

This study has determined the possible effects of sodium sulfate hot corrosion of SiC fiber-reinforced CAS glass-ceramic matrix composites and they are as follows:

- Corrosion of the SiC/CAS composite at 900° C is significant in the presence of sodium sulfate and an oxidizing atmosphere.
- Corrosion of the composite at 900° C in the presence of sodium sulfate in a non-oxidizing atmosphere (argon) is less severe and is limited to the matrix and fibers at or near the surface.
- Corrosion in samples coated in sodium sulfate at 900° C (air and argon) has lead to the formation of the following phases: Albite, Nepheline, Wollastonite, Rankinite, Pseudo-Wollastonite and Mullite.
- Corrosion in a non-oxidizing atmosphere at 900° C with a salt coating caused needle-like rankinite to be significantly reduced and pseudo-wollastonite, which is a low pressure high temperature polytype of $CaSiO_3$, forms vice wollastonite. Mullite also forms yet it was not present in the sample treated in air.
- Glassy phase effects were observed in the matrix as well as reacted phases.
- No significant fiber or matrix corrosion was observed in the uncoated sample heat treated in air at 900° C.
- These corrosion effects on the SiC/CAS properties are consistent with the findings of Wang, Kowalik and Sands [Ref. 15: pg. 11] as seen in Figure 11 which indicates a reduction in the mechanical properties due to hot corrosive effects. The major degradation occurs in the sample exposed to an oxidizing atmosphere and a lesser effect on the sample exposed to argon.

VII. RECOMMENDATIONS

The strength of a fiber/matrix composite is determined by its ability to transfer the load from the matrix to the fiber. The amount of load transferred is representative of the bond strength which in turn is greatly effected by the corrosion products as the fiber is degraded. This merits the examination of the fiber/matrix interface through the use of a Transmission Electron Microscope (TEM). The TEM may also be employed to investigate the mechanism for diffusion of corrosive products to the interior of the matrix. This is believed to occur along grain boundaries and could be verified with the use of the TEM.

The SiC fibers in this composite were uncoated which prevented an additional oxidation barrier against corrosion. The SiO_2 protective layer is not sufficient to withstand the hot corrosive effects of the sodium sulfate salts. A study is recommended to be conducted to determine whether a coating could be developed to reduce the extent of fiber degradation thus improving the mechanical properties after corrosion occurs.

It is also recommended that future studies be conducted on the monolith CAS system to determine corrosive effects on matrix constituents without the influence of the SiC fiber.

LIST OF REFERENCES

1. V.D. Frechette, L.D. Pye, J.S. Reed, Material Science Research, Plenum Press, 1974.

2. R.W. Kowalik, S. Wang, R.R. Sands, "Hot Corrosion Of Nicalon Fiber Reinforced Glass-Ceramic Matrix Composites: Microstructural Effects", Naval Air Warfare Center Technical Report, Warminster, PA, 1992.

3. D.R. Askeland, The Science and Engineering of Materials, PWS-Kent Publishing Co., 1989.

4. L.H. Van Vlack, "Physical Ceramics for Engineers", Addison-Wesley Publishing Co., Inc., 1964.

5. S.M. Bleay, V.D. Scott, b. Harris, R.G. Cook, F.A. Habib, " Interface Characterization and Fracture of Calcium Aluminosilicate Glass-Ceramics Reinforced with Nicalon Fibers", Journal of Material Science, Vol 27, 1992.

6. R.F. Cooper, K. Chyung, "Structure and Chemistry of Fibre Matrix Interfaces on Silicon Carbide Reinforced Glass-Ceramic Composites: An Electron Microscopy Study", Journal of Material Science, Vol 22, 1987.

7. S.W. Wang, A. Parvizi-Majidi, "Experimental Characterization of the Tensile Behavior of Nicalon Fiber Reinforced Calcium Aluminosilicate Composites", Journal of Material Science, Vol 27, 1992.

8. I.M. Daniel, G. Anastassopolous, J.W. Lee, "The Behavior of Ceramic Fiber Composites Under Longitudinal Loading", Composites Science and Technology, Vol 46, 1993.

9. K.K. Chawla, Composite Materials Science and Engineering, Springer-Verlang, 1987.

10. A.G. Evans, D.B. Marshall, "The Mechanical Behavior of Ceramic Matrix Composites", Acta Metallurgica, Vol 37, 1989.

11. M.H. Lewis, V.S.R. Murthy, "Microstructural Characterization of Interfaces in Fiber-Reinforced Ceramics", Composites Science and Technology, Vol 42, 1991.

12. N.S. Jacobson, "Corrosion of Silicon Based Ceramics in Combustion Environments", Journal of American Ceramic Society, Vol 76, 1993.

13. B.E. Deal, A.S. Grove, "General Relationship for the Oxidation of Silicon", Journal of Applied Physics, Vol 36, No. 12, 1965.

14. R. Bianco, N. Jacobson, "Corrosion of Cordierite Ceramic by Sodium Sulfate at 1000°C", Journal of Material Science, Vol 24, 1989.

15. S.W. Wang, R.W. Kowalik, R.R. Sands, "Hot Corrosion of Two Nicalon Fiber Reinforced Glass-Ceramic Matrix Composites", Ceramic Engineering and Science Proceedings, Vol 14 (7-8), 1993.

16. S.W. Wang, Private Conversation, 1994.

17. H. Salmang, Ceramics Physical and Chemical Fundamentals, Butterworth Publishing, 1961.

INITIAL DISTRIBUTION LIST

		No. Copies
1.	Defense Technical Information Center Cameron Station Alexandria VA 22304-6145	2
2.	Library, Code 052 Naval Postgraduate School Monterey CA 93943-5002	2
3.	Professor M.D. Kelleher, Code ME/Kk Chairman Department of Mechanical Engineering Naval Postgraduate School Monterey CA 93943-5000	1
4.	Professor Alan G. Fox, Code ME/Fx Mechanical Engineering Department Naval Postgraduate School Monterey CA 93943-5000	2
5.	Curricular Officer, Code 34 Department of Naval Engineering Naval Postgraduate School Monterey CA 93943-5000	1
6.	LT Peter J. Newton 114 Hoyt Lane Port Jefferson NY 11777	5
7.	Dr. Shaio-Wen Wang Code 6063 Aircraft Division Naval Air Warfare Center Warminster PA 18974	1
8.	Dr. Jeff Waldman Code 6063 Aircraft Division Naval Air Warfare Center Warminster PA 18974	1